

Designing a Framework for Solving Multiobjective Simulation Optimization Problems

Tyler H. Chang¹ and Stefan M. Wild²

¹Mathematics and Computer Science Division, Argonne National Laboratory,, 9700 S Cass Ave Bldg 240, Lemont, IL, USA 60439, tchang@anl.gov

²Applied Mathematics and Computational Research Division, Lawrence Berkeley National Laboratory,, 1 Cyclotron Rd, Berkeley, CA, USA 94720, wild@lbl.gov

July 7, 2023

Abstract

Multiobjective simulation optimization (MOSO) problems are optimization problems with multiple conflicting objectives, where evaluation of at least one of the objectives depends on a black-box numerical code or real-world experiment, which we refer to as a simulation. This paper describes the design goals driving the development of the parallel MOSO library ParMOO. We derive these goals from the research trends and real-world requirements that arise when designing and deploying solvers for generic MOSO problems. Our specific design goals were to provide a customizable MOSO framework that allows for exploitation of simulation-based problem structures, ease of deployment in scientific workflows, maintainability, and flexibility in our support for many problem types. We explain how we have achieved these goals in the ParMOO library and provide two examples demonstrating how customized ParMOO solvers can be quickly built and deployed in real-world MOSO problems.

Keywords: multiobjective optimization, simulation optimization, engineering design optimization, surrogate modeling, open-source software design

1 Introduction and Motivation

Multiobjective optimization problems (MOOPs) are optimization problems involving two or more potentially conflicting objectives. Such problems arise in numerous fields of science, with examples such as multidisciplinary engineering design [1, 2], scientific model calibration [3], high-performance computing (HPC) library autotuning [4], particle accelerator design [5], neural network architecture search [6, 7, 8], and computational chemistry [9, 10]. In such problems the goal is to find a set of “good” points from a design space with respect to a vector-valued objective function $\mathbf{F} : \mathcal{X} \rightarrow \mathbb{R}^o$. Here, \mathcal{X} is called the feasible design space and is typically assumed to be a compact subregion of \mathbb{R}^n . In this paper we assume each objective $F_i(\mathbf{x})$ is bounded from below so that the feasible objective space $\mathbf{F}(\mathcal{X})$ is lower bounded in each dimension. In the standard formulation, one seeks to minimize each objective (i.e., component of \mathbf{F}), a problem that is written as

$$\min_{\mathbf{x} \in \mathcal{X}} \mathbf{F}(\mathbf{x}). \quad (1)$$

Since it is typically not possible to find one $\mathbf{x} \in \mathcal{X}$ that simultaneously minimizes all o components of \mathbf{F} , the solution to (1) is generally a set of design points and corresponding objective values. Rather than describe when an objective value corresponds to a solution for (1), it is easier to begin by describing when an objective value does *not* correspond to a solution. An objective value $\mathbf{F}(\mathbf{x}) \in \mathbf{F}(\mathcal{X})$ is said to be dominated if there exists a $\mathbf{y} \in \mathcal{X}$ such that $\mathbf{F}(\mathbf{y}) \leq \mathbf{F}(\mathbf{x})$. Here we use the vector-inequality “ \leq ” to indicate that $\mathbf{F}(\mathbf{y})$ is componentwise less than or equal to $\mathbf{F}(\mathbf{x})$ with strict inequality $F_i(\mathbf{y}) < F_i(\mathbf{x})$ in at least one component

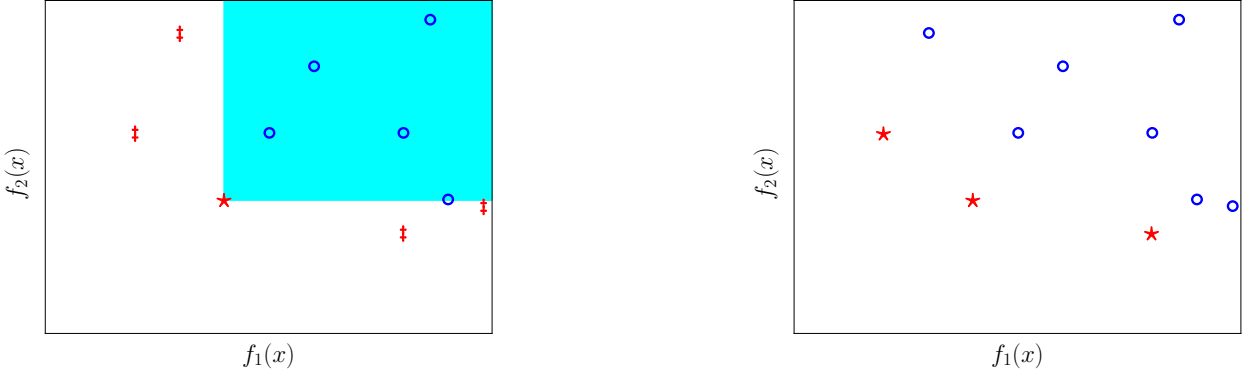


Figure 1: Left: The objective value $\mathbf{F}(\mathbf{x}^*)$ (labeled \star) dominates all objective values (with examples labeled \circ) in the shaded cone $\{\mathbf{v} \in \mathbb{R}^o : \mathbf{F}(\mathbf{x}^*) \leq \mathbf{v}\}$, while the objective values outside the cone (e.g., those labeled \ddagger) are not dominated by $\mathbf{F}(\mathbf{x}^*)$. Right: The objective values labeled \star are nondominated with respect to all other objective values (labeled \circ) in the dataset.

i. Conversely, an objective value $\mathbf{F}(\mathbf{x}^*)$ is said to be nondominated in a set of objective values $\Omega \subset \mathbb{R}^o$ if for all $\mathbf{F}(\mathbf{y}) \in \Omega$, $\mathbf{F}(\mathbf{y}) \not\leq \mathbf{F}(\mathbf{x}^*)$. The dominance relationship is illustrated in Figure 1.

If $\mathbf{F}(\mathbf{x}^*)$ is nondominated in $\mathbf{F}(\mathcal{X})$, then $\mathbf{F}(\mathbf{x}^*)$ is said to be Pareto optimal for (1), and \mathbf{x}^* is said to be efficient for (1). The set of all Pareto optimal objective values typically forms a $(o - 1)$ -dimensional trade-off surface, called the Pareto front (along a subset of the boundary of $\mathbf{F}(\mathcal{X})$). For further details on general MOOPs, we refer readers to the book by Ehrgott [11]. In general, a design point and objective value pair $(\mathbf{x}^*, \mathbf{F}(\mathbf{x}^*))$ are in the solution set for (1) if they are efficient/Pareto optimal. In a typical multiobjective optimization application, a *decision maker* uses a multiobjective optimization solver to identify a subset of all Pareto optimal objective values and select one or more of these as the preferred solution(s) based on domain expertise and personal preference.

A large class of real-world MOOPs consists of those derived from expensive numerical simulations [12, 4, 5, 1, 2], computer experiments [4, 6, 7, 8], and real-world experiments [13, 14, 9, 10]. We refer to such problems as multiobjective simulation optimization (MOSO) problems. Typically, the objectives in a MOSO problem are treated as black-box processes, and the problems are solved by using black-box optimization techniques [15]. Furthermore, since these simulations may be expensive to evaluate, MOSO algorithm performance is typically measured in terms of solution accuracy per number of total simulation evaluations. In this paper we focus on designing solvers for MOSO problems, which means that we exclude techniques that rely on access to derivatives of the simulations and/or require excessive numbers of simulation evaluations. Consequently, here we use the convention that “simulation” refers to an expensive black-box function that yields only zeroth-order information.

In this paper we describe the design considerations that drive the development of the parallel MOSO library ParMOO [16], which implements a framework based on surrogate modeling of black-box simulations. Unlike previous surrogate-based MOSO software, we focus on support for generic surrogate models, utilizing structure-exploiting methods and accommodating diverse scientific problems and workflows. We begin by deconstructing surrogate-based MOSO solvers into a system of simpler modules for performing tasks that are common across many different solver architectures. We then present an abstract framework for integrating these modules, while hiding unnecessary complexities, managing both raw simulation and objective data and parallel simulation evaluations. To demonstrate ParMOO’s effectiveness in exploiting real-world problem structures, we also provide access to two computationally inexpensive benchmark problems exhibiting such structures. These problems are easy to test on, since the expensive simulations have been replaced by machine learning models trained on real-world datasets.

The remainder of the paper is organized as follows. In Section 2 we review existing techniques, problem types, trends, and software in MOSO, and we describe the technical challenges and trade-offs involved in building a general-purpose MOSO library that achieves all of our design goals. In Section 3 we introduce our

framework for addressing these challenges. We then present two case studies that demonstrate the flexibility and power of our framework: Section 4 involves the calibration of a physics model, and Section 5 involves the design of material in a wet-lab environment. We conclude in Section 6 with a short discussion of our results.

2 Background and Design Principles

We now lay out the primary goals and requirements when designing a general framework for implementing modern surrogate-based MOSO algorithms. These goals and requirements depend on an understanding of the current state-of-the-art techniques and modern trends in MOSO, so we begin by reviewing these.

In addition to the techniques laid out in this paper, we acknowledge the existence of other special-purpose solvers and variations of the MOSO problem. In this work, however, we do not consider solvers that are tied to a specific application, such as neural architecture search [8] and chemical experiment design [10], or solvers that target other variations of the problem (1), including online multiobjective optimization [17] and multiobjective reinforcement learning [18]. We also acknowledge that a similarity exists between surrogate-based MOSO and active learning [19], which we consider to be a more generic problem than surrogate-based MOSO, the latter being more similar to multiobjective Bayesian optimization [20, 21, 6, 10].

2.1 Types of Algorithms for Multiobjective Simulation Optimization

Many algorithms have been proposed for solving MOSO problems. In general, these fall into three classes:

- *a priori* methods, where the decision maker expresses preferences for a particular solution *before* solving the problem;
- *a posteriori* methods, where the decision maker expresses preferences for a particular solution *after* solving the problem; and
- *interactive* methods, where the decision maker updates the preferences during the course of the optimization process.

For a summary of all three approaches in the context of multidisciplinary design optimization (MDO) problems, see the survey by Marler and Arora [22].

Among these three broad classes, *a priori* methods have historically been the most common in industrial-grade engineering tools [23] and modeling languages [24]. Such methods do not require dedicated multiobjective optimization solvers, however, since the decision maker’s preferences can typically be used to scalarize the problem *a priori*, allowing for the usage of a single-objective optimization solver. Therefore, these techniques are not the focus of this paper. Interactive methods are effective in situations where the decision maker cannot express preference *a priori* but gains an understanding of their preference during the course of the run [25]. Effective implementation of these techniques requires human-in-the-loop software, which is difficult to implement effectively (especially in a scientific workflow) and is beyond the scope of this paper. Therefore, although we briefly mention approaches to *a priori* and *interactive* multiobjective optimization, we focus primarily on *a posteriori* methods.

For the purpose of this paper we further divide *a posteriori* methods into three broad categories, which are common in the literature:

- multiobjective evolutionary algorithms (MOEAs), which extend single-objective evolutionary algorithms by using multicriteria ranking and selection processes;
- multiobjective directional search techniques, which extend deterministic algorithms for searching the design space, including multiobjective extensions of dividing rectangles (DIRECT), direct multisearch techniques, and multidirectional line-search techniques; and
- multiobjective extensions of Bayesian optimization techniques, which use a multiobjective acquisition function (discussed more in the next section).

For a recent survey focusing on *a posteriori* MOSO algorithms, see [26].

2.2 Common Techniques for Multiobjective Optimization

Several techniques are particularly prevalent in a posteriori MOSO algorithms.

Scalarization is a “classical” technique in multiobjective optimization, which is still prevalent in many modern MOSO algorithms and applications. Scalarization is the process of collapsing a MOOP into a single-objective subproblem that can be (approximately) solved to produce a single (approximately) efficient/Pareto optimal solution. A scalarization is defined by a scalarization function $A : \mathbb{R}^o \rightarrow \mathbb{R}$, such that

$$\arg \min_{\mathbf{x} \in \mathcal{X}} A(\mathbf{F}(\mathbf{x})) \in \arg \min_{\mathbf{x} \in \mathcal{X}} \mathbf{F}(\mathbf{x}).$$

The scalarized problem $\min_{\mathbf{x} \in \mathcal{X}} A(\mathbf{F}(\mathbf{x}))$ can be solved by using any derivative-free optimization method; for a recent survey of such methods, see [27].

One commonly used scalarization technique is the weighted sum scalarization

$$A(\mathbf{F}(\mathbf{x})) = \mathbf{w}^T \mathbf{F}(\mathbf{x}) = \sum_{i=1}^o w_i F_i(\mathbf{x}),$$

where $\mathbf{w} \geq \mathbf{0}$ are called the scalarization weights [11, Chapter 3]. Other common scalarization techniques include the epsilon-constraint method [11, Chapter 4], Pascoletti–Serafini scalarization [28], the reference point method [29], quadratic scalarization schemes [30], and expected hypervolume improvement [31, 32]. In an a priori method, the decision maker may provide some fixed set of scalarization functions, which are carefully selected to target only the desired solution point(s). In an a posteriori method, however, each of the above-mentioned approaches would need to be combined with some *adaptive scheme* [33, 34, 28, 35] for sweeping through different members in a family of scalarization functions, thus producing numerous solution points covering the Pareto front. Evaluating the performance of any one of these scalarization schemes is nontrivial, but it is generally agreed that a good scheme should produce solution points that are on or close to the true Pareto front, offer good coverage of the entire Pareto front, and are well distributed [36, 37].

For MOSO problems where simulation evaluations are expensive, the total problem expense can get out of hand if too many simulation evaluations are required. Therefore, modern MOSO solvers often reduce the need for true simulation evaluations by combining one or more of the above-mentioned evolutionary or direct search algorithms with a computationally cheaper surrogate model [38, 37, 39, 40, 41]. Here, each component of an expensive-to-evaluate objective $\mathbf{F}(\mathbf{x}) = (F_1(\mathbf{x}), \dots, F_o(\mathbf{x}))$ is modeled by a computationally cheaper surrogate function $\hat{F}_1 \approx F_1, \dots, \hat{F}_o \approx F_o$. Several “candidate solutions” can then be suggested by finding points that are efficient/Pareto optimal for the surrogate problem

$$\min_{\mathbf{x} \in \mathcal{X}} (\hat{F}_1(\mathbf{x}), \dots, \hat{F}_o(\mathbf{x})). \quad (2)$$

When \mathbf{F} is sufficiently more expensive to evaluate than $\hat{F}_1, \dots, \hat{F}_o$ (in terms of computational time and resources), the cost of finding (approximately) efficient/Pareto optimal points for (2) can be much less than the cost of finding such points for (1). In practice, these surrogates could be any of a variety of classical approximation or machine learning [42] models.

One of the common frameworks from the statistics literature for solving computationally expensive optimization problems (including MOOPs) by using surrogate models is the response surface methodology (RSM) [14]. In an RSM-based method, the optimization algorithm uses the following iterative process (as illustrated in Figure 2) to solve a MOSO problem.

1. Generate and evaluate a design-of-experiments for all of the objective functions.
2. Fit surrogates to each objective function using the data gathered from evaluating the design, and then solve several scalarizations of the surrogate problem in (2) to generate a batch of candidate design points (i.e., design points that are approximately efficient for the surrogate problem).
3. Evaluate the candidate design points and use the new data to update the surrogate models.
4. Iterate between steps 2 and 3 until the problem (1) has been solved to sufficient accuracy or the computational budget has been exhausted.

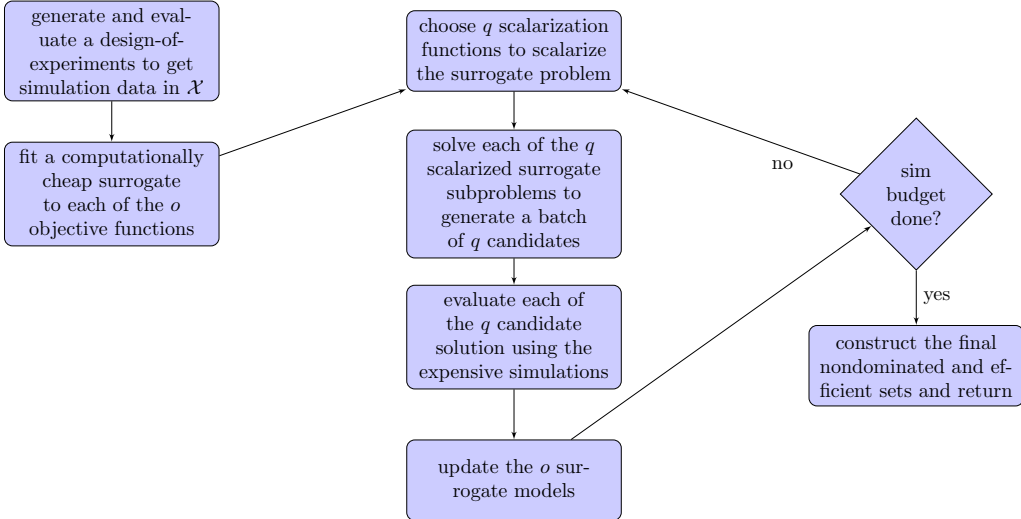


Figure 2: Flowchart for the RSM framework, when applied for solving MOSO problems.

A special case of surrogate modeling consists of Gaussian process models, which also provide statistical uncertainty information. Such a statistical surrogate can be combined with a multiobjective acquisition function to form multiobjective Bayesian optimization solvers [43, 20, 44, 45]. We view multiobjective acquisition functions as a generalization of the multiobjective scalarization functions discussed above, in the sense that an acquisition function may require additional data beyond just raw objective values, such as surrogate model parameters. For this reason, to be as general as possible, we use the term “acquisition function” when describing our framework, instead of “scalarization function.”

To our knowledge, currently no flexible, extensible, open-source software exists for implementing solvers for generic MOSO problems in a general-purpose RSM framework. The reason is partially because of the complexity of managing interactions between advanced simulation, modeling, and optimization tools, especially when multiple simulations, data sources, and/or surrogates are involved. In order to alleviate the complexity of these interactions, integration between such techniques is often handled through a large library integrating numerous such capabilities; examples include Dakota [46], PETSC with TAO [47, 48], and FUN3D’s integrated optimization tools [23]. In application areas such as MDO, entire libraries of predefined surrogate models with common interfaces [42] have been developed, alongside MDO-specific platforms [49, 50, 51] for managing the complexity of integrating optimizers, surrogates, and simulations. In other areas such as neural architecture search [8] and chemical engineering [10], domain-specific optimization tools have been created that reduce complexity by focusing on a single problem class.

2.3 Design Principles for Multiobjective Simulation Optimization

We now summarize several advanced challenges in building software for MOSO problems.

First, in the area of surrogate modeling, state-of-the-art techniques in various domains are able to efficiently integrate observational data with theory-driven models and constraints to provide improved accuracy [52]. Accommodating these highly customized models, however, requires a highly customizable framework for surrogate modeling and optimization of surrogate models. Along similar lines, customized strategies for static design of experiments [53], dynamic sampling [54], and optimal sampling [19] have long been popular

and can have dramatic effects on model accuracy, particularly for regions of interest. Therefore, support for highly customizable initial search strategies and dynamic data acquisition techniques are also important in a truly customizable framework for RSM-based methods.

Design goal #1: We want to provide a highly customizable software framework for building and deploying RSM-based MOSO solvers, allowing for interoperable usage of generic and highly customizable search techniques, surrogate models, acquisition functions, and optimization solvers.

Similar to customizing our surrogate models, depending on how the outputs of the simulation are used, we can build custom derivative-free optimization solvers to exploit known structures in how the simulation outputs are used to formulate the objective. For example, in the single-objective case, one can exploit a least-squares [55] or other composition-based [56] structure in the objective definition by using a custom solver. In the multiobjective case, such structures could be even more diverse. For example, many multi-objective problems are *heterogeneous* in the sense that certain objectives may be computationally expensive to evaluate and offer no known structure, while others are computationally cheap to evaluate and have derivative information readily available [37, 41]. To exploit structures such as these, we need to provide our optimization solvers with access to any structures in our objective definitions.

Design goal #2: We want to structures in how the simulation outputs are used (such as composition with an algebraic function) to be visible to the optimization solver. To our knowledge, no existing multiobjective framework does this.

Another challenge in simulation optimization is achieving parallel simulation evaluations. Some existing optimization solvers provide parallelism through a single paradigm (e.g., Python multiprocessing, OpenMP, or MPI) [57, 39, 58]. However, this does not provide sufficient flexibility for usage in a wide variety of modern HPC systems. In cases where the “simulation” is a true numerical simulation performed on an HPC system, we may need to exploit various modern architectures, including GPU-based [59] and neuromorphic computing systems [60, 61]. Thus, performance portability has become increasingly important in modern simulation software [62, 63], and solvers with a single inflexible parallelism backend will not be appropriate for next-generation hardware. Similarly, we seek to include experimentation-based applications where the “simulation” is actually a physical experiment that must be carried out in a wet-lab environment [13].

In order to address these issues, many platforms [64, 13] and libraries/frameworks [65, 66] have been created for coordinating parallel evaluations, complex simulations, data storage, and heterogeneous resource utilization. Additionally, domain-specific tools for managing simulation, modeling, and optimization interplay also manage distribution over parallel resources [50]. However, effectively utilizing these platforms is nontrivial if the optimization software was not originally designed with mindfulness for these paradigms [67, 68]. Therefore, there is a need for software that provides parallelism and simulation environment flexibility.

Design goal #3: We want to make our framework easy to deploy in a wide variety of modern scientific workflows. Doing so requires flexibility in how simulation evaluations are distributed, integrability with multiple parallel/distributed backends, and data management such as logging and checkpointing.

Another modern requirement stems from a need to improve findability, accessibility, interoperability, and reusability of both scientific data [69] and software [70]. In the case of software, this goes hand in hand with maintainability, continuous development practices, and reduced technical debt through better open-source scientific software practices, such as agile methodology, continuous integration, and automated testing [71]. Note that many new and similar libraries are adopting such practices [65, 72], and several existing multiobjective optimization libraries have recently been refactored to become more agile [73, 74].

Design goal #4: Our software framework and workflow must be easy to use, maintain, and extend. In particular, this includes usability by nondomain experts, extensibility to add novel and highly customized solvers, and agility to adapt to applications in previously unforeseen circumstances.

2.4 Existing MOSO Software

Several open-source multiobjective solvers and libraries exist. The majority of available software implements MOEAs. Widely used MOEA-based solvers include ParEGO [21], which also integrates Gaussian process surrogate modeling, and SPEA2 [75]. Another MOEA that has perhaps been the most widely used multiobjective optimization algorithm for the past 20 years is the nondominated sorting genetic algorithm II (NSGA-II) [76]. NSGA-II and other common MOEAs are implemented in numerous libraries, including Platypus [77], pymoo [57], PlatEMO [78], jMetal/jMetalPy [79, 74], and pagmo/pygmo [80]. The framework DEAP [81] is also frequently used for implementing distributed evolutionary algorithms in Python, including distributed MOEAs.

Several open-source software packages also exist for direct search methods. Notable individual solvers include MODIR [12], which implements a multiobjective DIRECT solver integrated with a multiobjective line search program; the serial and parallel solvers in VTMOP [39], which utilize RSM together with adaptive weightings and trust-region methods; and the serial or parallel solver BiMADS, which is limited to biobjective problems and is included in the larger framework NOMAD v3 [58]. BoostDFO is a MATLAB package containing a library of parallel solvers [82], and PyMOSO [83] is a Python framework that is targeted primarily at integer-valued problems.

In recent years several Bayesian optimization libraries and frameworks have emerged, supporting multiobjective optimization. Since we can consider Bayesian optimization as a special case of RSM, these tools are of particular interest. The Python library Dragonfly [6], for instance, was designed for solving neural architecture search problems but can be applied to generic multiobjective Bayesian optimization problems. Perhaps most relevant to our goals in this paper is the BoTorch [43] framework for implementing and deploying parallel, production-ready, generic Bayesian optimization (including multiobjective) algorithms, while layering over the automatic differentiation PyTorch framework [84].

Analyzing these developments, we note that the most widely used multiobjective optimization software in recent years all support any combination of real (continuous-valued), discrete (i.e., integer-valued), and/or categorical (nonordinal) variables and support both constrained and unconstrained problems [43, 74, 80, 57, 6, 58]. For a generic surrogate-based optimization solver, supporting mixed-variable problems and domain-specific input spaces provides the additional challenge of modeling functions of mixed variables. However, it is extremely important to a modern package’s usability. Even more recently, several applications of multiobjective Bayesian optimization have utilized custom distance functions and problem embeddings, which allow for optimization over non-Euclidean design spaces [6, 10]. We foresee that as these embeddings become more prevalent, it will become increasingly necessary to utilize them for optimization, thus adding another layer of complexity to surrogate modeling and optimization.

Design goal #5: We want to be flexible in our support for a wide variety of problem types. This includes support for mixed-variable problems, customized latent space embeddings, and types of constraints.

Considering the above classifications and criteria, we present a list of solvers and libraries in Table 1, along with our novel software library ParMOO, whose motivation is described in this paper. We acknowledge that many of these software packages are under active development and may add features in the future, so we base our classifications by the documented features at the time of this publication.

2.5 Design Goals

For convenience, we briefly restate the five design goals and summarize the overall challenges in building a software framework to our specifications.

- G1. We want to provide a highly customizable software framework for building and deploying RSM-based MOSO solvers.
- G2. We want to give the optimization solver access to any available structure in how the simulation outputs are used to define the objectives.
- G3. We want to make our framework easy to deploy in a wide variety of modern scientific workflows.

Name	Type	Language	Method	Constr.	Var. Types	Surrogates
BiMADS	S	C++	MS	yes	mixed	yes
BoostDFO	L	Matlab	MS	some	real	yes
BoTorch	L	Python	BO	yes	mixed	yes
DEAP	L	Python	EA	yes	mixed	no
DESDEO	L	Python	any	yes	real	yes
Dragonfly	L	Python	BO	yes	mixed	yes
jMetal	L	Java	EA	yes	mixed	no
jMetalPy	L	Python	EA	yes	mixed	no
MODIR	S	Fortran	MS	no	real	no
ParEGO	S	C	EA/BO	no	real	yes
pagmo	L	C++	EA	some	mixed	no
ParMOO	L	Python	MS/BO	yes	mixed	yes
PlatEMO	L	Matlab	EA	some	mixed	some
Platypus	L	Python	EA	yes	mixed	no
pygmo	L	Python	EA	some	mixed	no
pymoo	L	Python	EA	some	mixed	no
PyMOSO	L	Python	MS	yes	int	no
SPEA2	S	C	EA	no	real	no
VTMOP	S	Fortran	MS	no	real	yes

Table 1: Examples of general-purpose open-source software for MOSO problems. The “Type” column indicates whether the software is an individual solver (S) or library of solvers (L); the “Language” column specifies the primary programming language that the software was written in; the “Method” column specifies whether the software primarily uses evolutionary algorithms (EA), Bayesian optimization (BO), or multi-directional search (MS) methods; the “Constr.” column indicates whether the software supports nonlinear constraint specification; the “Var. Types” column indicates the types of variables that the software supports; and the “Surrogates” column indicates whether the software includes or supports the usage of surrogate models.

G4. Our software framework and workflow must be easy to use, maintain, and extend.

G5. We want to be flexible in our support for a wide variety of problem types.

G1 is somewhat of an engineering challenge; however, it requires some thought in how one decomposes RSM-based MOSO solvers into a generic framework, which can be implemented cleanly in Python. G2 and G5 are more research questions, requiring novel structures and abstractions to make unforeseen problem structures and embeddings visible to the user. G3 and G4 are, by themselves, engineering problems. However, maintaining these engineering requirements while implementing our other design goals requires consideration of how to balance solver flexibility against software complexity.

3 A Framework for Multiobjective Simulation Optimization

We now outline our framework for solving multiobjective optimization problems. In particular, we describe how this framework addresses the design goals and challenges laid out in Section 2.5. The framework is implemented in the software library ParMOO [16], which can be obtained by following the installation instructions in its online documentation [85].

3.1 An Object-Oriented Modular Design

Despite the level of complexity necessary to achieve G1, the biggest engineering challenge of this work is maintaining the design goals G3 and G4. To do so, we focus on a modular design, where each module addresses a particular component of the requirements from G1 and where all modules share a common

interface. The natural paradigm for implementing such a framework is object-oriented programming (OOP). To this end, we have implemented abstract base classes (ABCs) for each of the solver components. We have also implemented a **MOOP** class that utilizes implementations of these ABCs in an RSM framework. A unified modeling language (UML) diagram outlining how the **MOOP** class depends on these ABCs is shown in Figure 3. Referring back to G1, the four primary ABCs for ParMOO are

- the **GlobalSearch** class, which abstracts the interface for utilizing adaptive sampling or static design-of-experiments techniques;
- the **SurrogateFunction** class, which abstracts the interface for fitting a generic surrogate model;
- the **AcquisitionFunction** class, which abstracts the interface for implementing a scalarizing acquisition function; and
- the **SurrogateOptimizer** class, which accepts a scalarized, differentiable or non-differentiable function during initialization and uses the appropriate methods to solve the scalarized surrogate problem.

To allow nonexperts to utilize ParMOO without implementing each of these techniques, we provide a built-in library of implementations for several standard techniques from each of the categories. With respect to G3, the advantages of this object-oriented approach are as follows:

- this allows the maintainers of ParMOO to easily extend its functionality and test these changes independently of the overall framework;
- this allows optimization, machine learning, and engineering researchers to separately study and test the performance of novel methods for sampling, surrogate modeling, data acquisition, and surrogate problem optimization; and
- this allows users to build customized solutions to their problem, based on a combination of their own domain knowledge and general advice from the optimization community and our documentation, without worrying about low-level details, such as how various components of a solver should integrate and which techniques are compatible with each other.

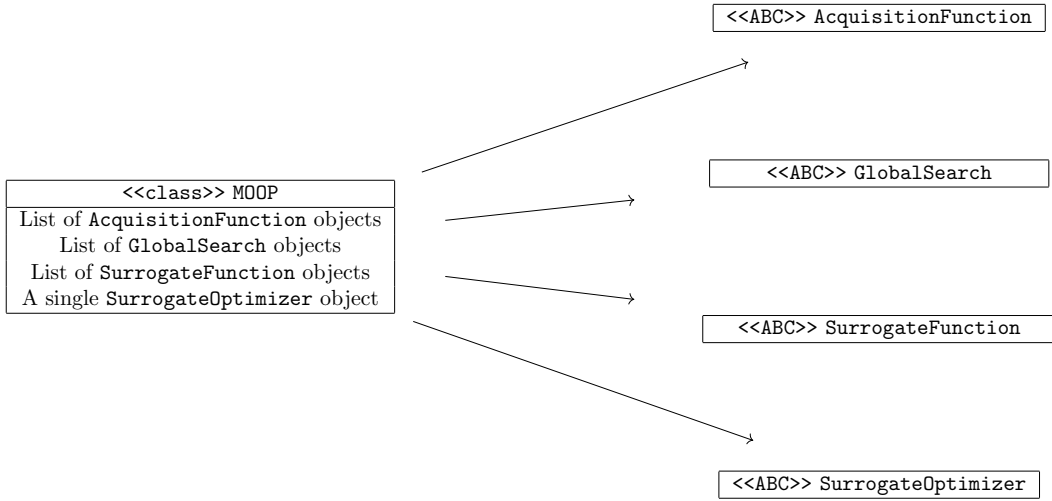


Figure 3: UML diagram outlining the dependencies between the **MOOP** class and the ABCs defining the MOSO solver's components.

The **MOOP** class itself is also highly modular, with clearly documented methods for performing low-level tasks, and is easily extensible. Developers can easily overwrite certain functionality, such as the method that

distributes expensive simulation evaluations, in order to adapt to novel architectures and use cases. In this way, the modular OOP framework also addresses G4.

The downside of this approach is that the object-oriented interface adds an additional level of complexity, similar to that of learning a new modeling language, such as JuMP [86] or Pyomo [24]. It also requires users to become aware of the basic components of an RSM-based multiobjective solver, in order to correctly utilize our library of components and framework. Ultimately, this mental overhead is significantly greater than that required to learn to properly utilize other Python libraries of multiobjective solvers, such as pymoo [57] and pagmo/pygmo [80]. However, we believe that this approach is a necessary compromise in order to achieve G1, G2, and G5 as laid out in Section 2.5.

In this way, ParMOO is not comparable to many of the libraries and individual solvers listed in Table 1. Of these software packages, ParMOO is perhaps most comparable to DEAP [81] and BoTorch [43], which implement similar frameworks for solving slightly different classes of problems using different classes of techniques.

3.1.1 Supporting Local Methods for Black-Box Optimization

It is well-known that compared to global model-based approaches such as Bayesian optimization, *local* model-based methods (such as trust-region methods) are much more scalable for high-dimensional design spaces [87]. A significant challenge when designing *local* model-based solvers is maintaining a quality interpolation set during the course of optimization, through an occasional *geometry improving* step and careful *trust-region radius* control [27, 72]. In Figure 3, we do not explicitly list a module for geometry improvement and trust-region radius control. Indeed, knowing when to take a geometry improving step or decrease/expand the trust region can be slightly more challenging in the context of multiobjective optimization than in the single-objective case. Since the scalarization can change between iterations, it is not easy to keep track of when a model’s geometry has “gone stale” or when its trust region is too small/large.

In ParMOO, local model geometry is a property of the `SurrogateFunction` class, and it is the job of each `SurrogateFunction` implementation to determine its current trust-region radius when queried (this can return the radius of the entire design space for global modeling methods) and also to provide a rule for local geometry improvement. In the library of provided `SurrogateOptimizer` implementations, there are several local optimizers, which will regularly query the `SurrogateFunction` class’s `setCenter` method to re-center the surrogate model at the current iterate and request the current trust-region radius. These methods will then only solve the surrogate optimization problem from inside the current trust region. Furthermore, whenever the `SurrogateOptimizer` returns a candidate design that has already been observed, ParMOO will treat this as a “failed iteration,” which automatically triggers a call to the `SurrogateFunction` class’s `improve` method. The `improve` method should return a local or global model-improving candidate.

These techniques have been used to successfully build structure-exploiting local solvers using trust regions and geometry improvement, as described in Section 4.

3.2 Distinguishing between Simulations, Objectives, and Constraints

The next challenge that we need to address directly is G2, which requires making visible to an optimization solver how the simulation outputs are used. Our key insight here is to manage and model simulation outputs separately from objective values and constraint penalties. Figure 4 shows how we traditionally view MOOPs, with \mathbf{F} mapping directly from the feasible design space into the feasible objective space. Figure 5 shows how ParMOO treats MOOPs, with a black-box simulation function \mathbf{S} mapping into an intermediate “simulation output space” \mathcal{S} , before \mathbf{F} maps $\mathcal{X} \times \mathcal{S}$ into the feasible objective space.

The abstraction depicted in Figure 5, while simple, has been shown to be powerful in its ability to model problem structures and save simulation evaluations [88]. Two specific problem structures that we highlight here are sum-of-squares structure and heterogeneous objectives.

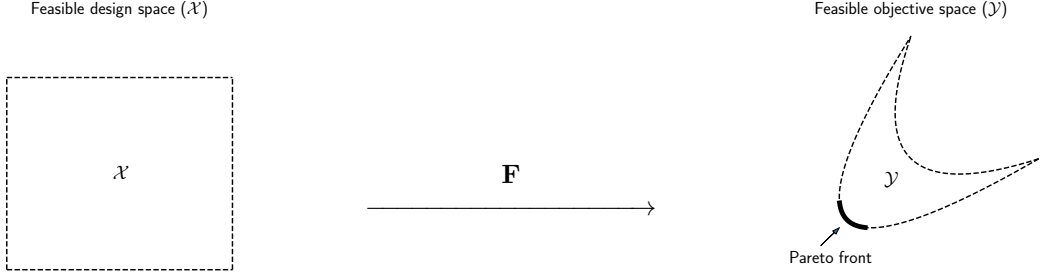


Figure 4: The feasible design space \mathcal{X} (left) is mapped directly to the feasible objective space \mathcal{Y} (right) via the vector-valued objective function \mathbf{F} .

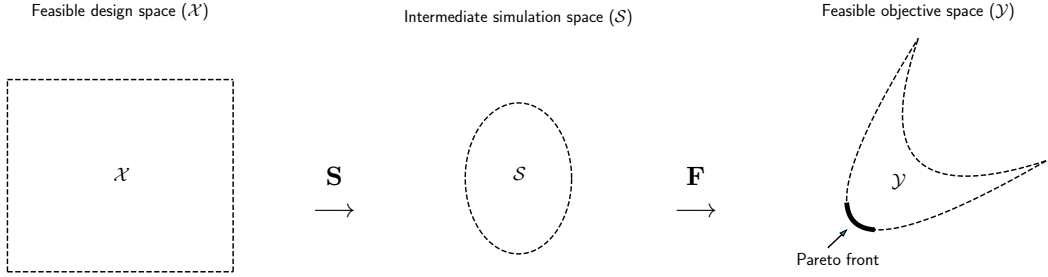


Figure 5: The feasible design space \mathcal{X} (left) is mapped into an intermediate simulation output space \mathcal{S} (center) via the black-box simulation \mathbf{S} , then to the feasible objective space \mathcal{Y} (right) via the algebraic objective function \mathbf{F} .

3.2.1 Exploiting Sum-of-Squares Structure

A sum-of-squares structure occurs when one or more objective functions $F_i(\mathbf{x})$ is calculated as

$$F_i(\mathbf{x}) = \sum_{j \in J} \mathbf{S}(\mathbf{x})^2, \quad (3)$$

where J is an index set for the simulation outputs $1, \dots, m$.

The principle behind exploiting the sum-of-squares structures in the single-objective case is detailed in [89]. Assuming that the objective F_i is twice continuously differentiable, for any surrogate model $\hat{\mathbf{S}}(\mathbf{x})$ that models $\mathbf{S}(\mathbf{x})$, if $\hat{\mathbf{S}}(\mathbf{x})$ interpolates $\mathbf{S}(\mathbf{x})$ for all previously evaluated \mathbf{x} and under some mild geometric assumptions about the spacing of Ξ , then the resulting approximation $\hat{F}_i(\mathbf{x}) = \sum_{j \in J} (\hat{S}_i(\mathbf{x}))^2$ has some second-order accuracy “for free” [89], even when $\hat{\mathbf{S}}(\mathbf{x})$ has only first-order accuracy. Therefore, when solving any single-objective formulation of the problem, the local convergence of the resulting model-based optimization algorithm can be superlinear.

In the case of MOSOs, it is unclear how these convergence guarantees will generalize since there is no standard definition of convergence rate in the multiobjective case. However, one can easily construct solvers that exploit the structure (3), as in [55], by applying a trust-region-constrained surrogate to the outputs of \mathbf{S} and solving the MOOP using a trust-region-based solver. An example is provided in Section 4.

3.2.2 Exploiting Heterogeneous MOOPs

A heterogeneous MOOP is a MOSO problem with heterogeneous objectives, such that one or more objectives are derived from the simulation outputs, while other objectives are cheap to evaluate and have readily

available gradient information [37, 41]. To solve these problems efficiently, we need to take advantage of black-box techniques such as surrogate modeling when optimizing for the expensive objective(s), but the cheap objective should not be modeled using complex surrogates since they are simple to evaluate and may even have obvious minima. Although such structures exist in numerous real-world problems [41], they are either not easy or impossible to exploit in existing MOSO solvers [37].

In ParMOO, the computationally expensive objectives are defined by using the simulation outputs in \mathcal{S} . However, the cheap objectives are defined by a direct mapping from \mathcal{X} , which does not use the intermediate outputs in \mathcal{S} . In this way, ParMOO is able to directly control the computationally cheap objectives and will evaluate them many times when solving the surrogate optimization problems. However, ParMOO will still exercise restraint in true evaluations of the expensive objectives, relying heavily on their surrogate models. An example is provided in Section 5.

3.3 Managing Complexity through Problem Embeddings

To address G5, we need to handle problems involving continuous, integer-valued, and categorical variables, as well as nonlinear constraints. However, many methods for doing so require problem-specific techniques or heavy modification to the structure outlined in Section 3.1. To maintain usability and maintainability (G4), we must be careful in the techniques that we use.

Ultimately, for handling mixed variables, our method of choice is to embed the problem into a continuous “latent space” and then solve a relaxation of the problem. Variations of this technique are used in many optimization software tools. For example, the surrogate modeling toolbox pySMT [42] handles categorical variables by using a one-hot encoding and then uses its surrogate models to relax the problem. In the case of material design, EDBO [10] uses the molecular descriptor calculator Mordred [90] to calculate a three-dimensional descriptor for various molecule networks and then solves a Bayesian optimization problem in this latent space.

Similarly, ParMOO abstracts this idea by creating a hidden embedding layer for handling mixed variables; see Figure 6. Upon input, (1) all categorical variables are embedded into a continuous latent space, (2) all embedded design variables and other design variables are rescaled into a normalized range, and (3) all variables taking on discrete values are relaxed. After ParMOO solves the surrogate optimization problem, all candidate design points are extracted from the latent space back into the ambient space and binned to their nearest legal values if necessary. ParMOO provides a default embedding for categorical variables, which utilizes a one-hot encoding, followed by multiple correspondence analysis on the enumeration of all legal encodings to identify the lowest-dimensional latent space that preserves all information, as described in Section 3.3.1. However, this technique is not scalable to a large number of categorical variables. Therefore, for complex problems, ParMOO also allows users to provide a custom embedding procedure.

The primary advantage of this approach is that it maintains a level of simplicity and maintainability regardless of the problem type. There is no need to use customized search, surrogate modeling, or optimization techniques for solving mixed-variable problems (although doing so may improve performance) since the default techniques are designed to operate on the rescaled latent space. The flexibility to accept a custom embedding tool is also useful for domains such as molecular engineering, where these tools are available [90].

A similar approach is taken for handling nonlinear constraints. Following the progressive barrier approach used in [5], we formulate a single penalty function that aggregates the violation of all constraints, and we apply it to the objective behind the scenes, dynamically adjusting the penalty parameters until ParMOO suggests only candidate points whose values (or predicted-values, when constraints are based on simulation outputs) are feasible. Again, this approach allows us to use generic bound-constrained optimization tools to solve the surrogate problems, without requiring special tools to handle nonlinear constraints.

3.3.1 The Default Problem Embeddings

When users are not able to provide a domain-specific custom embedding for their application, a general-purpose embedding is needed. One common approach that is used for model-based optimization in many different settings is one-hot encoding of categorical variables [91, 92]. A major drawback of this approach is that one-hot encodings greatly increase the dimensionality of the design space by creating an additional “artificial variable” for each level of each category. Therefore, many state-of-the-art surrogate modeling

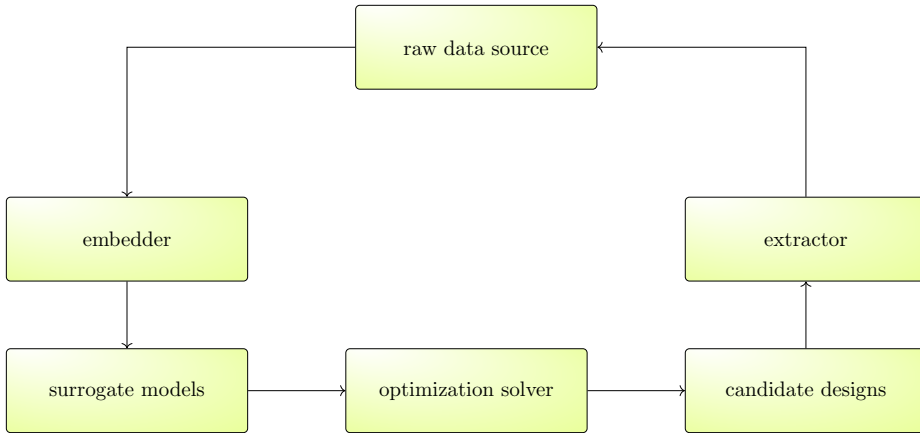


Figure 6: An embedding layer is used to take inputs of mixed-variable types and denormalized ranges and produce continuous variables in the range $[0, 1]$, which can be modeled by a generic surrogate and tuned by a generic bound-constrained optimization solver.

libraries prefer other techniques, such as mixed-variable distance kernels in the context of RBF and Gaussian process modeling [92].

In ParMOO, since the default embedding needs to be compatible with many different classes of surrogates, a one-hot encoding (plus continuous relaxation) is preferable. However, in order to avoid creating an excessive number of redundant categories, ParMOO enumerates the one-hot encodings for every valid setting of categorical variables as rows of a “codex” matrix $A^{(\text{cat})}$. Then, ParMOO applies principle component analysis to eliminate redundant and unused categories. This is achieved by subtracting the mean value from each column of $A^{(\text{cat})}$, and then calculating its singular-value decomposition $U\Sigma V^\top$. If Σ has rank r , then the first r rows of V^\top define an embedding into a r -dimensional latent space, where ParMOO will perform continuous optimization on surrogate-relaxed categories. The resulting relaxed value can be extracted through V and binned to the nearest valid one-hot encoding after the result of the optimization.

Although preferable to a generic one-hot encodings, this approach is still not scalable to large numbers of categorical variables. In such cases, a custom embedding will still be needed.

3.4 Flexibility and Extensibility to Novel Workflows

G3 was to make our framework flexible enough that it is easy to deploy in a variety of scientific workflows. Key examples include HPC and wet-lab environments.

To achieve this goal, we have designed ParMOO to issue simulation evaluations exclusively via the wrapper function `MOOP.evaluateSimulation()`, which is exclusively called from within the solver routine `MOOP.solve()`. In situations where only the simulation command must be changed for integration with existing workflow technology, this can be achieved by extending the `MOOP` class and overwriting the `MOOP.evaluateSimulation()` method. In other situations, where control over the frequency with which simulation evaluations are distributed is required (for example, when batching simulation evaluations), the entire `MOOP.solve()` method can be overwritten.

This has been demonstrated in ParMOO’s `libE_MOOP` class, which extends the `MOOP` class and overwrites the `solve` method to dynamically distribute simulation evaluations on HPC systems using the libEnsemble library [65, 66]. Although overwriting the `solve` method is not entirely trivial, it is considerably less work than the effort needed to integrate other solvers that were not originally designed with extensibility in mind [67]. ParMOO’s libEnsemble interface is the recommended method for achieving scalable parallelism with ParMOO.

3.5 The Resulting Framework

Putting everything together, we present our framework for solving MOSO problems as implemented in ParMOO. To create a MOOP object, the user begins by specifying a solver for the surrogate problems and a dictionary of hyperparameters. Next, the user must add problem details, including

- n design variable dictionaries, each specifying a design variable for the problem and a custom embedder routine, if applicable;
- s simulation dictionaries, each defining a simulation/data source for the problem, plus the number of intermediate outputs (m_i), the search technique used to sample that simulation’s output space, and the surrogate function used to model that simulation’s output;
- o objective dictionaries, each specifying an algebraic function that can be used to calculate the objective values from the design variables and simulation outputs and (optionally) the gradient of that objective;
- p constraint dictionaries, identical to the objective dictionaries but for the purpose of evaluating constraint violations; and
- q acquisition dictionaries, each specifying an acquisition function that can be used to scalarize the problem, where q also determines the batch size for parallel evaluations.

A UML diagram outlining this framework is shown in Figure 7. Note that only the relevant public methods discussed in this section are shown. In the MOOP class’s implementation, several additional public and private helper methods are included, as well as additional “setter” methods to facilitate saving, loading, logging, and checkpointing [85].

4 Case Study: Solving a Multiobjective Inverse Problem

In this section we apply ParMOO to a multiobjective inverse problem, where the goal is to tune the parameters of the Fayans energy density functional (EDF) model based on experimental data. This problem is fully described in [3]. The forward model is expensive to evaluate and not publicly available. Therefore, to maintain reproducibility of results, we optimize a synthetic problem based on a neural network model that was trained on the dataset from [3].

4.1 Background on Fayans EDF Calibration

We now review important aspects of the Fayans EDF calibration. Let $S_{\mathbf{x}} : s \rightarrow t$ denote the Fayans EDF model. A single forward evaluation of $S_{\mathbf{x}}$ accepts a normalized parameter vector $\mathbf{x} \in \mathbb{R}^{13}$ and an input s and produces a physical observation t . Given 198 observational data pairs $(s_1, t_1), \dots, (s_{198}, t_{198})$, the goal of the Fayans EDF model calibration is to find “good” parameter vectors $\mathbf{x}^* \in \mathbb{R}^{13}$ such that $S_{\mathbf{x}^*}(s_i) \approx t_i$ relative to a given standard error $\sigma_i > 0$ for $i = 1, \dots, 198$.

In traditional Fayans EDF calibration, it is assumed that all observations have been normalized by the standard errors σ such that they have equal and independent normalized errors. It is then reasonable to minimize the χ^2 loss across all 198 observations via the single-objective formulation

$$\min_{\mathbf{x} \in \mathbb{R}^{13}} \sum_{i=1}^{198} \left(\frac{S_{\mathbf{x}}(s_i) - t_i}{\sigma_i} \right)^2. \quad (4)$$

In [3], however, it is noted that the contributions to the χ^2 loss may vary across 9 different observational types. Since the 9-objective formulation is prohibitively expensive to solve, we consider a simplified three-objective formulation, where related observational types are combined, leaving just three observational classes. This allows us to define the following multiobjective formulation of the Fayans EDF calibration:

$$\min_{\mathbf{x} \in \mathbb{R}^{13}} F_{\mathbf{x},j}, \quad j = 1, 2, 3, \quad (5)$$

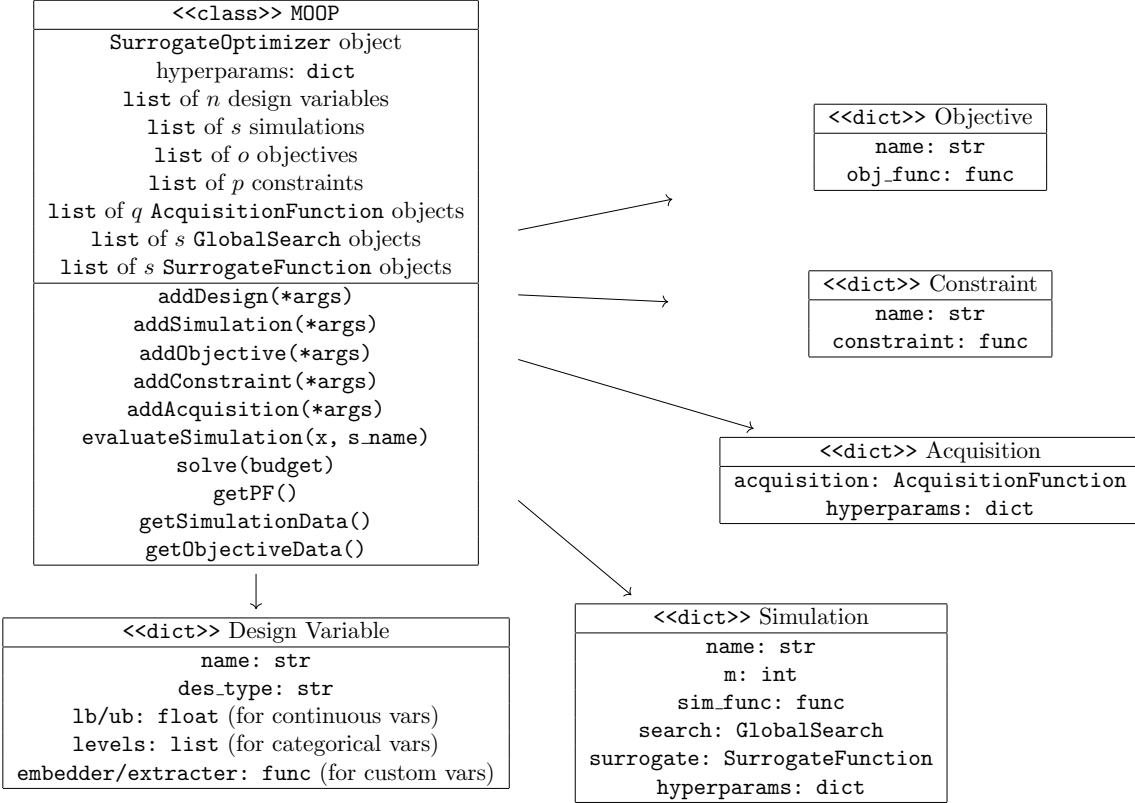


Figure 7: UML diagram outlining the key dictionaries, components, and methods that make up a MOOP object and its contents.

where $F_{\mathbf{x},j} = \sum_{i \in \Phi_j} \left(\frac{S_{\mathbf{x}}(s_i) - t_i}{\sigma_i} \right)^2$ and Φ_1, Φ_2, Φ_3 is a partitioning of $\{1, \dots, 198\}$ based on the three observational classes described above.

In this paper we solve the multiobjective formulation of the Fayans EDF calibration problem (5). In this problem, evaluation of the forward model for all 198 observations $[S_{\mathbf{x}}(s_1), \dots, S_{\mathbf{x}}(s_{198})]$ is viewed as a single computationally expensive black box. The three loss functions $F_{\mathbf{x},j}$ ($j = 1, 2, 3$) all have sum-of-squares structure, which can be exploited by an optimization solver as discussed in Section 3.2.1.

4.2 The Neural Network Residual Model

For our experiments, since $S_{\mathbf{x}}$ is expensive and we strive for reproducibility, we fit a multilayer perceptron (MLP) to approximate the standardized residual functions $R_i(\mathbf{x}) = \frac{S_{\mathbf{x}}(s_i) - t_i}{\sigma_i}$, $i = 1, \dots, 198$. We do this using a dataset of labeled observations for the residual functions $R_1(\mathbf{x}), \dots, R_{198}(\mathbf{x})$ for 52,079 distinct values of \mathbf{x} . This dataset was gathered by [3] and, as described in that paper, comes from running multiple starting design points with several different single-objective solvers on the single-objective formulation of the problem (4). Therefore, we note that the dataset is not uniformly distributed and has increased density in the neighborhood of several local solutions to the single-objective problem (4).

The primary challenge when training the MLP used in this section is ensuring that the prediction accuracy is high for optimal values of the multiobjective problem (5). In particular, large regions of the parameter space were determined to be unstable for the single-objective formulation, and therefore no observational data is available. Additionally, within the stable region, for several values of i , the observational data for $R_i(\mathbf{x})$ could range in magnitude from less than 1 to over 10^{20} . While prediction errors that are greater than 1 in magnitude would be acceptable (and expected) for these large residuals, it is essential for our fidelity

to the original problem that we maintain prediction errors on the order of 10^{-2} in the neighborhood of the true solutions.

To handle infeasible regions of the parameter space where no observational data is available, we impose bound constraints for ParMOO, following the constraints given by [3], shown in Table 2. To handle the wide range on observational values, we apply a double-logarithmic transformation to large values of $R_i(\mathbf{x})$, followed by a tanh transformation. Because this collapses huge error values, this transformation ensures that, during training, the MLP places much higher importance on matching observations where the residual function $R_i(\mathbf{x})$ has a low score.

Variable Name	Lower Bound	Upper Bound
ρ_{eq}	0.146	0.167
E/A	-16.21	-15.50
K	137.2	234.4
J	19.5	37.0
L	2.20	69.6
h_{2-}^v	0.0	100.0
a_+^s	0.418	0.706
h_∇^s	0.0	0.516
κ	0.076	0.216
κ'	-0.892	0.982
f_{ex}^ξ	-4.62	-4.38
h_+^ξ	3.94	4.27
h_∇^ξ	-0.96	3.66

Table 2: Upper and lower bounds on the stable region for the parameter space for the Fayans EDF model $S_{\mathbf{x}}(s)$, as reported by [3]. We have access to observational data only in these ranges, and therefore the trained MLP will be accurate only within these bounds.

For the network architecture, we define an MLP with 13 inputs, 198 outputs, and 2 hidden layers, with 256 nodes per layer. We then apply tanh activation functions for every layer of the network (including the output layer) and train the network using the transformed data defined above. For validation, we first stratify the complete observational database by low/high residuals across all three observational classes defined in (5) and then withhold 5% of the data across all stratifications for our validation set. The network was trained in `keras` [93] using 5,000 epochs of RMS-prop. We verify that the trained model obtains low relative error across all stratified residual ranges in the validation set. Most importantly, after descaling the outputs to their original ranges, on the bottom stratification where the residuals are lowest in magnitude across all three observational classes, we obtain a mean absolute error (MAE) of just 0.036 on the validation set, which is acceptable accuracy for this problem.

In the remainder of this section we use the trained `keras` model described above as a synthetic representation of the original Fayans EDF calibration problem.

4.3 Exploiting Structure in ParMOO

The sum-of-squares structure and how it can be exploited have been previously outlined in Section 3.2.1. In typical software implementations of this strategy [55], special care is taken to ensure that all geometric conditions on the interpolation nodes hold, thus requiring the algorithm to occasionally take geometry-improving evaluations and using a sequence of local (trust-region) approximations, as described in Section 3.1.1. In ParMOO’s built-in `LocalGaussRBF` surrogate model implementation, the trust-region radius is adaptively chosen based on the distance to the $(n + 1)$ th nearest neighbor of the current iterate. Then, whenever the solution to the trust-region-constrained surrogate problem fails to produce a sufficient decrease in the scalarized objective value, ParMOO’s default model-improving step is triggered, which draws a random sample from a distribution whose variance is highest in directions of low variance in the current data set. This policy satisfies the standard model geometry criteria with probability one.

Furthermore, since we are solving a multiobjective formulation of the problem and not a single-objective formulation, special care must be taken when interpreting how “superlinear local convergence” would translate in the multiobjective case. We will see empirically, however, that simply modeling $\mathbf{R}(\mathbf{x})$ separately from $\mathbf{F}(\mathbf{x})$ greatly accelerates the practical convergence of our structure-exploiting multiobjective solver.

4.4 The ParMOO Fayans EDF Solvers

To demonstrate its ability to utilize parallel function evaluations (as we would need to if we were evaluating the true Fayans EDF model instead of our synthetic MLP model), we use ParMOO’s `libEnsemble` interface to distribute simulation evaluations with a batch size of 10. This is achieved by using 9 epsilon-constraint acquisition functions and one fixed weighting, where the fixed weights are even across all three observational classes. This fixed weighting encourages ParMOO to also solve the single-objective formulation, since it is equivalent to the χ^2 loss. To define the problem, we create a `libEMOOP` object in ParMOO and add 13 continuous design variables, with names and bounds as given in Table 2.

To define a structure-exploiting variant as described in the preceding section, we then add a single simulation function that models all 198 components of our synthetic MLP residual function using local trust-region-(LTR-) constrained Gaussian radial basis function (RBF) models and initializes its observational database using a 2,000-point Latin hypercube sample (LHS). We next add three differentiable algebraic objective functions, which calculate the sum of squares from the simulation outputs across each of the three different observational classes. Then, to allow ParMOO to focus on interesting regions of the design space where none of the observational classes result in terrible performance, we add three nonlinear constraints, each enforcing that the squared residuals in a particular observable class should not exceed $10 \times$ its optimal values reported in [3]. ParMOO then solves the surrogate optimization problems within the LTR using the L-BFGS-B [94] implementation in SciPy [95].

To compare with the performance when the structure is not exploited, as would be the case with other existing multiobjective software, we define a “black-box” variation of this problem. For the black-box variant, the 198-output simulation described above was replaced by a 3-output “black-box” simulation, where the sum of squares has already been computed across all three observational classes. Then, for each objective, we provide an identity map from each simulation output to each objective. Otherwise, we define the problem equivalently as with the structured variant.

In both cases, ParMOO is then run for 800 iterations. Since we begin with a 2,000-point LHS search and provide a batch size of 10 points per iteration, this results in a total budget of 10,000 simulation evaluations for each solver. We note that for a typical simulation optimization problem, this budget of 10,000 simulation evaluations is unrealistically large. In fact, because of the complexity of our Gaussian RBF surrogate models and cost of solving the surrogate optimization problem, for this large a budget our iteration costs are extremely high. However, it is worth running to such a large simulation budget in order to understand the solver’s performance in the limit.

Note that because of the complexity of solving the surrogate optimization problem and the nonnegligible cost of evaluating the `keras` model, such a solve requires a substantial amount of compute time. To account for randomness in the LHS searches and scalarization weight initializations, we perform 5 runs of each solver and average the performance.

For reproducibility, this entire experimental setup, including the trained MLP that was used as a synthetic problem representation, is available at <https://github.com/parmoo/parmoo-solver-farm/tree/main/fayans-model-calibration-2022>. Note that for ease of use and compatibility reasons, we have transferred our `keras` model’s weights into an equivalent `torch` model [84], and this is reflected in the GitHub repository.

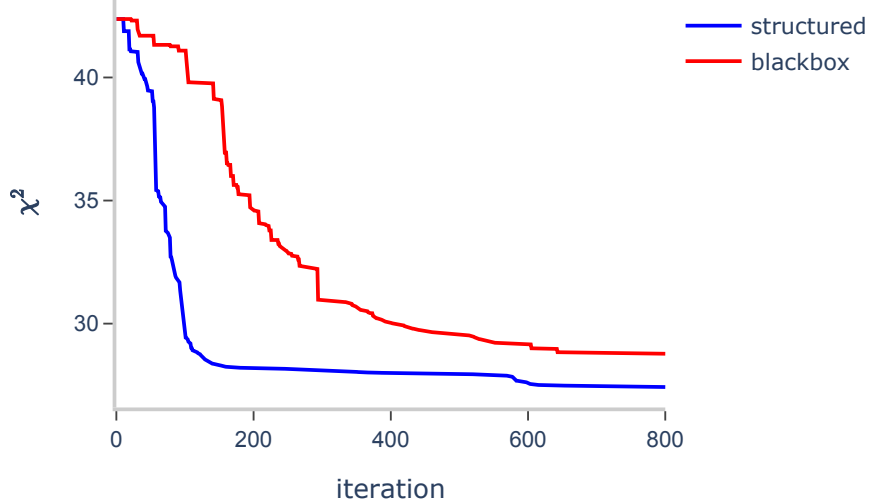
4.5 Results

The results of solving (5) based on the `keras`/`torch` residual model are presented here. In order to account for variability resulting from randomness in the initial design-of-experiments, all performance results have been averaged across five random seeds. First, borrowing the metric used in [3], we present the χ^2 loss across all observable classes in Figure 8. Note that for χ^2 loss, small values are better. Next, to estimate

the multiobjective performance of our methods, we present a rescaling of the widely used hypervolume performance indicator [36] in Figure 9. For the hypervolume indicator, large values are better.

Note that the hypervolume indicator is extremely sensitive to problem scaling and the choice of Nadir point, so its raw values are difficult to interpret. In an effort to normalize values, we present the improvement in hypervolume over that of the initial 2,000-point LHS design, as a percentage of the hypervolume dominated by that original design. Even after this normalization, however, the absolute value of the hypervolume improvement is still difficult to interpret since it is still influenced by the total hypervolume between the true Pareto front and Nadir point. In Figure 9 we see less than a 0.7% increase in total hypervolume. This is because our Nadir point is determined by the lower-bound constraints that ParMOO enforced on the range of interesting values, which were intentionally set to be overly pessimistic. However, the hypervolume improvements of the two methods relative to each other can still be taken as an indicator of relative performance.

Figure 8: Iteration vs. χ^2 loss when solving the Fayans EDF calibration with ParMOO, both exploiting the sum-of-squares structure (structured) and with a standard (black-box) approach. The total simulations used by the end of iteration I are calculated as $2000 + 10I$.



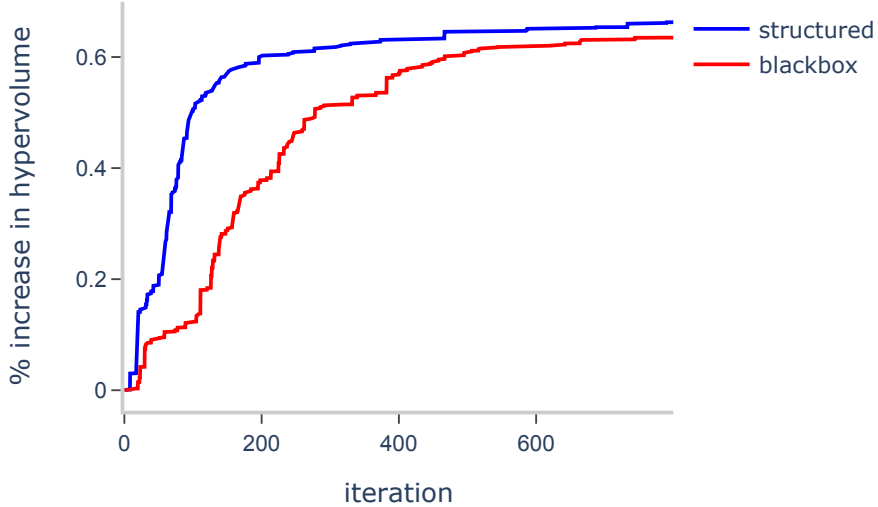
For both the χ^2 loss and hypervolume improvement, the structured solver converges considerably faster than does the black-box solver. With respect to the χ^2 loss, in just 200 iterations (4,000 simulation evaluations) the structured solver achieves better performance than the black-box solver will in all 800 iterations (10,000 simulation evaluations). This result is to be expected: since one of our acquisition functions specifically targets this solution with fixed scalarization weights, ParMOO behaves similarly to how a structure-exploiting single-objective solver would for this performance metric.

With respect to the percent hypervolume improvement (a true multiobjective performance metric), the ParMOO’s structured solver also achieves significantly improved performance. However, the convergence appears to be slightly slower than for the χ^2 loss. This is to be expected since solving the full multiobjective problem is considerably harder than solving a single scalarization. However, especially for limited computational budgets, the performance of the structured solver is still dramatically improved.

5 Case Study: A Multiobjective Chemical Design

To demonstrate ParMOO’s effectiveness with heterogeneous objectives and flexibility to support diverse scientific workflows, in this section we apply ParMOO to solve a materials engineering problem. Here, two of the three objectives are derived from a continuous-flow chemistry experiment that is conducted in a

Figure 9: Iteration vs. percentage hypervolume improvement when solving the Fayans EDF calibration with ParMOO, both exploiting the sum-of-squares structure (structured) and with a standard (black-box) approach. The total simulations used by the end of iteration I are calculated as $2000 + 10I$.



wet-lab environment, while the third objective is algebraic. As in Section 4, to make our results open and reproducible, in this section we use a nonlinear model of the chemical response surface, based on real-world data collected using nuclear magnetic resonance (NMR) spectroscopy on the solutions from a continuous-flow reactor (CFR).

5.1 Background on CFR Material Design

In material manufacturing applications, our goal is to propose a technique for chemical manufacturing that can be used to produce a desired material with high purity at scale. In particular, in this application we are manufacturing the electrolyte 2,2,2-trifluoroethyl methyl carbonate (TFMC) by mixing one of two predetermined potential solvents with one of two predetermined potential bases. Note that for confidentiality reasons, we do not include the true names of these potential solvents and bases in this section; they are simply labeled as S1, S2 and B1, B2, respectively. This does not affect the reproducibility of our results since they are also labeled as such in the nonlinear model that we used to represent the problem in this section.

Our goal is to find an optimal pairing of solvents and bases and conditions (such as reaction time, equivalence ratio, and temperature) for producing a pure solution of TFMC in a CFR. However, in addition to producing a pure solution, we want to be able to use short reaction times, so that we can produce large quantities of TFMC at scale. We expect that this will require us to use higher temperatures, which could activate a side reaction and produce an unwanted byproduct, thereby reducing the purity.

5.2 The Chemical Response Surface Model

In the context of ParMOO, this problem has three continuous design variables and two categorical design variables. These variable names and their ranges/potential values are given in Table 3. The response values of interest are the integrals of TFMC and byproduct production values over a fixed-length time window, as measured by using NMR spectroscopy.

Since we cannot provide access to the CFR for our experiments, in this section we use a nonlinear response surface representing the physical continuous-flow chemistry experiment. These models were fit by using real-world data that was collected by providing a physical CFR/NMR setup as a simulation that ParMOO could query in closed loop. To do so, ParMOO’s extensible interface was layered over the MDML tool [13], which

Variable Name	Var. Type	Lower Bound	Upper Bound	LegalVals.
temperature (T)	continuous	35 C	150 C	N/A
reaction time (RT)	continuous	60 sec	300 sec	N/A
equiv. ratio (EQR)	continuous	0.8	1.5	N/A
solvent	categorical	N/A	N/A	S1,S2
base	categorical	N/A	N/A	B1,B2

Table 3: Variable types, bounds, and legal values for the CFR material optimization problem discussed in this section. Note that continuous variables have bounds, while categorical variables have legal values.

uses an Apache kafka backend to distribute requests for experiment evaluations to the CFR and collects and returns NMR results directly to an online database that ParMOO can query for simulation results. For more information on how this data was collected, see [96], which describes the collection of a smaller dataset by using an identical experimental setup.

After a budget of 62 experiments, ParMOO had converged on several approximate solutions to the real-world problem, and it was no longer economically viable to continue the real-world experiment since the cost of real-world materials is nonnegligible. The resulting experimental database of design point/integral-value pairs was used in this section to fit the nonlinear models described above. Since this dataset is relatively sparse in the 5-dimensional input space, special care was taken to ensure that the resulting model does not exhibit non-physical behaviors. In particular, to verify our model, we have ensured that both of our response surfaces

- approximate the underlying data with low MAE, particularly for near-optimal design points;
- do not take on negative values anywhere in the feasible design space, which would be physically impossible since the outputs represent time integrals of material production;
- do not have a sum that exceeds the total amount of solvent and base provided for any inputs in the design space; and
- do not take unexpected maxima/minima along the boundaries of the design space, which could be an artifact of a lack of data in those regions, allowing our model to overextrapolate.

To achieve these criteria, we hand-crafted a small number of physically meaningful nonlinear terms for our response surface based on the expected chemistry of the reaction. We then fit the coefficients of these terms to each of the two integrals, by using a combination of generalized linear regression with `scikit-learn` [97]. The resulting MAE was found to be within the acceptable ranges. Using hyperparameter tuning with the `Powell` solver from `scipy.optimize.minimize` [95], we were also able to guarantee that the individual global minima for each model was nonnegative and the sum of the global maxima was within the acceptable range. We then verified that the individual minima and maxima for each model were located in acceptable regions of the design space, which agree with our physical intuition and empirical data.

In the remainder of this section we use these trained response surface models as the true chemical response surfaces for both the TFMC and byproduct integrals.

5.3 Heterogeneous Problem Structure

In this problems, two of the three objectives are the result of a true black-box experiment, which must be carried out in a wet-lab environment using real materials and with an extremely restrictive budget. However, the third objective represents the reaction time, which is one of the directly controllable inputs. Therefore, ParMOO is able to directly control this output, as described in Section 3.2.2, and is able to exploit this ability to accelerate its practical convergence.

5.4 The ParMOO CFR Material Design Solver

To define the problem, we provide ParMOO with the five design variables shown from Table 3, with their respective variable types and bounds/values. To handle the two categorical variables, we use ParMOO’s

default categorical variable embedder, which embeds the four distinct combinations of categorical variables into a three-dimensional continuous latent space. Combined with the three continuous design variables, this results in a six-dimensional effective optimization space.

For the structured variation of the problem, ParMOO is provided with the pretrained nonlinear model of the chemical response surface, described in Section 5.2. ParMOO is configured to treat this as a single simulation with two outputs, using a Latin hypercube sample (LHS) with 50 evaluations to produce the initial database and Gaussian RBFs for surrogate modeling. Next, ParMOO is given three objectives, two of which are identity mappings from the simulation outputs and the third of which is an identity mapping from the reaction time design variable. Then, two epsilon-constraint acquisition functions and one fixed-weighting are added, resulting in a batch size of three simulation evaluations per iteration.

For comparison and to demonstrate the advantage in exploiting the heterogeneous problem structure, we also provide an identical implementation of ParMOO for this problem, where the third “reaction time” objective is provided to ParMOO as a third black-box simulation output. This results in ParMOO modeling the third output as a black-box function and ignoring the heterogeneous structure, as would occur when using most other off-the-shelf multiobjective black-box optimization solvers. All other settings are identical as in the structured variation defined above.

One of the critical challenges of performing automatic experimentation in the context of material manufacturing is the cost of raw materials and performing real-world experiments. Although we do not have these costs for our computational model of the material response surface, we have run ParMOO with a restrictive budget of just a 50-point initial design followed by 30 iterations with 3 acquisition functions (140 total experiments). By exploiting the heterogeneous problem structure, we hope to still achieve good performance (especially for our cheap objective) with this limited budget.

The response surface model described above and the code for reproducing the experiments presented here are given at <https://github.com/parmoo/parmoo-solver-farm/tree/main/cfr-material-design-2022>. The results are presented in the next section.

5.5 Results

The results of tuning manufacturing conditions based on our chemical response surface are presented here. Again, all performance results have been averaged across 5 unique random seeds.

First, to assess our performance with respect to our one cheap objective, we present the average minimum observed reaction times (in seconds) subject to a 75% purity constraint in Figure 10. Note that for these reaction times, small values are better. Next, as in Section 4.5, we present the improvement in hypervolume as a proportion of the gap between initial hypervolume and total possible hypervolume (with respect to the ideal point) in Figure 11. Again, for the hypervolume improvement, large values are better.

As in Section 4.5, the structured solver greatly outperforms the black-box approach by both metrics. We note that although the time required to achieve over 75% conversion is a physically meaningful convergence metric and demonstrative of ParMOO’s ability to directly control the reaction time (the algebraic objective), this time we did not provide any fixed scalarization that would explicitly target this solution, reducing to a single-objective problem.

We note that ParMOO’s structure-exploiting solver achieves excellent performance on both this problem and the Fayans problem from Section 4.5 with little additional work from the user, even though these structures are considerably different.

6 Discussion and Continued Work

In this paper we have described the design principles behind the design of the MOSO library ParMOO. To summarize, our five main design goals are

1. customizability of solvers;
2. exploitation of structures in MOSO problems;
3. ease of use in scientific workflows;

Figure 10: Iteration vs. minimum reaction time that achieves at least a 75% conversion rate when solving the CFR chemical manufacturing problem with ParMOO, both exploiting the heterogeneous structure (structured) and with a standard (black-box) approach. The total simulations used by the end of iteration I are calculated as $50 + 3I$.

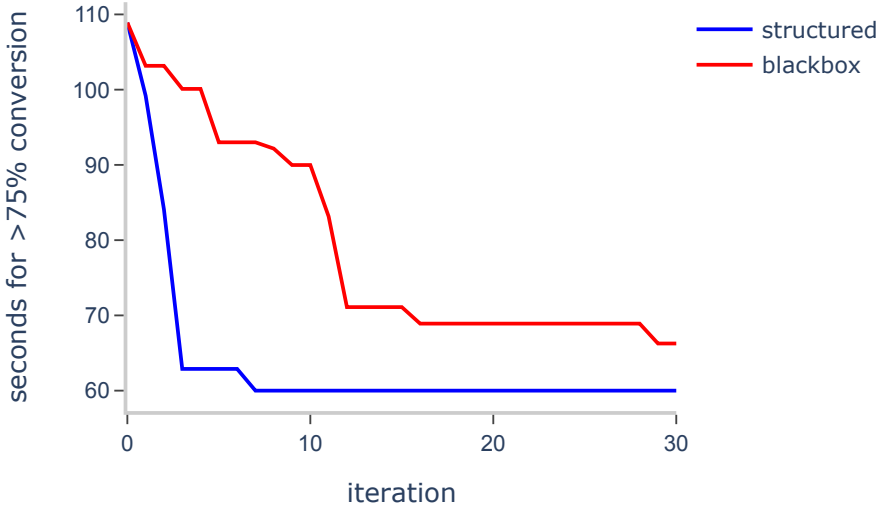
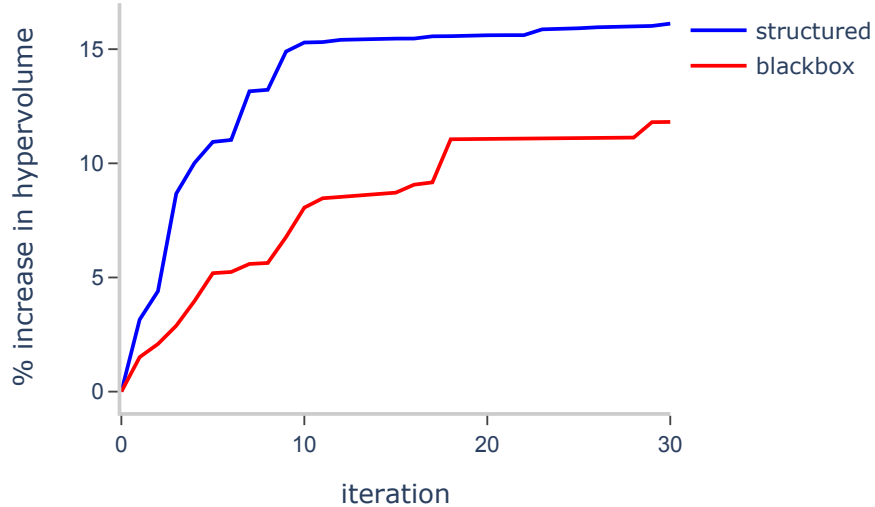


Figure 11: Iteration vs. percentage hypervolume improvement when solving the CFR chemical manufacturing problem with ParMOO, both exploiting the heterogeneous structure (structured) and with a standard (black-box) approach. The total simulations used by the end of iteration I are calculated as $50 + 3I$.



4. usability, extensibility, and maintainability as an open-source software package; and
5. flexibility in support for a wide variety of problem types.

We have achieved these goals through an object-oriented design that is highly modularized, utilizes an intermediate simulation output space, and embeds complex problems into a continuous latent input space.

This framework has been demonstrated on open-source models of two real-world problems, and these models and the code for reproducing our results have been shared through our `parmoo-solver-farm` repository <https://github.com/parmoo/parmoo-solver-farm>.

Although these two problems exhibit completely different structures, ParMOO is able to effectively exploit the structure in both cases and to considerably improve the convergence relative to that of a black-box approach that does not exploit known structure. Notably, defining such a structure-exploiting solver requires little additional work or customization from the user.

ACKNOWLEDGMENT

We are grateful to Jared O’Neal, Witold Nazarewicz, and Paul-Gerhardt Reinhard for providing the Fayans functional data and to Joseph Libera, Jakob Elias, Santanu Chaudhuri, and Trevor Dzwiniel for their respective roles in the acquisition of the CFR materials data. We are also grateful to Jeff Larson, John-Luke Navarro, and Steve Hudson for their advice on best practices in scientific software development and support in our usage of libEnsemble.

This work was supported in part by the U.S. Department of Energy, Office of Science, Office of Advanced Scientific Computing Research’s SciDAC program under Contract Nos. DE-AC02-05CH11231 and DE-AC02-06CH11357.

References

- [1] J. Sobieszcanski-Sobieski, A. Morris, M. Van Tooren, *Multidisciplinary Design Optimization Supported by Knowledge Based Engineering*, John Wiley & Sons, Ltd., Chichester, UK, 2015.
- [2] W. Zhao, R. K. Kapania, Multiobjective optimization of composite flying-wings with SpaRibs and multiple control surfaces, in: Proc. 2018 Multidisciplinary Analysis and Optimization Conference, AIAA, 2018, p. 3424. doi:10.2514/6.2018-3424.
- [3] R. Bollapragada, M. Menickelly, W. Nazarewicz, J. O’Neal, P.-G. Reinhard, S. M. Wild, Optimization and supervised machine learning methods for fitting numerical physics models without derivatives, *Journal of Physics G: Nuclear and Particle Physics* 48 (2020) 024001. doi:10.1088/1361-6471/ab009.
- [4] T. H. Chang, J. Larson, L. T. Watson, Multiobjective optimization of the variability of the high-performance LINPACK solver, in: Proc. 2020 Winter Simulation Conference (WSC 2020), IEEE, 2020c, pp. 3081–3092. doi:10.1109/WSC48552.2020.9383875.
- [5] N. Neveu, T. H. Chang, P. Franz, S. Hudson, J. Larson, Comparison of multiobjective optimization methods for the LCLS-II photoinjector, *Computer Physics Communication* 283 (2023). doi:10.1016/j.cpc.2022.108566.
- [6] K. Kandasamy, K. R. Vysyraju, W. Neiswanger, B. Paria, C. R. Collins, J. Schneider, B. Poczos, E. P. Xing, Tuning hyperparameters without grad students: Scalable and robust Bayesian optimisation with Dragonfly, *Journal of Machine Learning Research* 21 (2020) 1–27. URL: <http://jmlr.org/papers/v21/18-223.html>.
- [7] F. Karl, T. Pielok, J. Moosbauer, F. Pfisterer, S. Coors, M. Binder, L. Schneider, J. Thomas, J. Richter, M. Lang, E. C. Garrido-Merchán, J. Branke, B. Bischl, Multi-Objective Hyperparameter Optimization – An Overview, Technical Report, arXiv preprint, 2022. doi:10.48550/ARXIV.2206.07438.
- [8] M. Parsa, J. P. Mitchell, C. D. Schuman, R. M. Patton, T. E. Potok, K. Roy, Bayesian multi-objective hyperparameter optimization for accurate, fast, and efficient neural network accelerator design, *Frontiers in Neuroscience* 14 (2020) Article No. 667. doi:10.3389/fnins.2020.00667.
- [9] A. M. Schweidtmann, A. D. Clayton, N. Holmes, E. Bradford, R. A. Bourne, A. A. Lapkin, Machine learning meets continuous flow chemistry: Automated optimization towards the Pareto front of multiple objectives, *Chemical Engineering Journal* 352 (2018) 277–282. doi:10.1016/j.cej.2018.07.031.

[10] B. J. Shields, J. Stevens, J. Li, M. Parasram, F. Damani, J. I. M. Alvarado, J. M. Janey, R. P. Adams, A. G. Doyle, Bayesian reaction optimization as a tool for chemical synthesis, *Nature* 590 (2021) 89–96. doi:10.1038/s41586-021-03213-y.

[11] M. Ehrgott, *Multicriteria Optimization*, Lecture Notes in Economics and Mathematical Systems Series, 2 ed., Springer Verlag, Heidelberg, Germany, 2005. doi:10.1007/3-540-27659-9.

[12] E. F. Campana, M. Diez, G. Liuzzi, S. Lucidi, R. Pellegrini, V. Piccialli, F. Rinaldi, A. Serani, A multi-objective DIRECT algorithm for ship hull optimization, *Computational Optimization and Applications* 71 (2018) 53–72. doi:10.1007/s10589-017-9955-0.

[13] J. R. Elias, R. Chard, J. A. Libera, I. T. Foster, S. Chaudhuri, The manufacturing data and machine learning platform: Enabling real-time monitoring and control of scientific experiments via IoT, *2020 IEEE 6th World Forum on Internet of Things (WF-IoT)* (2020) 1–2. doi:10.1109/WF-IoT48130.2020.9221078.

[14] R. H. Myers, D. C. Montgomery, C. M. Anderson-Cook, *Response Surface Methodology: Process and Design Optimization Using Designed Experiments*, 4 ed., John Wiley & Sons, Inc., Hoboken, NJ, USA, 2016.

[15] C. Audet, W. Hare, *Derivative-free and blackbox optimization*, Springer Series in Operations Research and Financial Engineering, Springer International, Cham, Switzerland, 2017. doi:10.1007/978-3-319-68913-5.

[16] T. H. Chang, S. M. Wild, ParMOO: A Python library for parallel multiobjective simulation optimization, *Journal of Open Source Software* 8 (2023b) 4468. doi:10.21105/joss.04468.

[17] S. Mannor, V. Perchet, G. Stoltz, Approachability in unknown games: Online learning meets multi-objective optimization, in: *Proc. 27th Conference on Learning Theory (PMLR)*, volume 35 of *Proceedings of Machine Learning Research*, PMLR, Barcelona, Spain, 2014, pp. 339–355. URL: <https://proceedings.mlr.press/v35/mannor14.html>.

[18] C. F. Hayes, R. Rădulescu, E. Bargiacchi, J. Källström, M. Macfarlane, M. Reymond, T. Verstraeten, L. M. Zintgraf, R. Dazeley, F. Heintz, et al., A practical guide to multi-objective reinforcement learning and planning, *Autonomous Agents and Multi-Agent Systems* 36 (2022) 1–59. doi:10.1007/s10458-022-09552-y.

[19] T. P. Sapsis, A. Blanchard, Optimal criteria and their asymptotic form for data selection in data-driven reduced-order modelling with Gaussian process regression, *Philosophical Transactions of the Royal Society A* 380 (2022) 20210197. doi:10.1098/rsta.2021.0197.

[20] S. Daulton, M. Balandat, E. Bakshy, Differentiable expected hypervolume improvement for parallel multi-objective Bayesian optimization, *Advances in Neural Information Processing Systems* 33 (2020) 9851–9864. URL: <https://proceedings.neurips.cc/paper/2020/file/6fec24eac8f18ed793f5eaad3dd7977c-Paper.pdf>.

[21] J. Knowles, ParEGO: a hybrid algorithm with on-line landscape approximation for expensive multi-objective optimization problems, *IEEE Transactions on Evolutionary Computation* 8 (2006) 1341–66. doi:10.1109/tevc.2005.851274.

[22] T. R. Marler, J. S. Arora, Survey of multi-objective optimization methods for engineering, *Structural and Multidisciplinary Optimization* 26 (2004) 369–395. doi:10.1007/s00158-003-0368-6.

[23] R. T. Biedron, J. R. Carlson, J. M. Derlaga, P. A. Gnoffo, D. P. Hammond, W. T. Jones, B. Kleb, E. M. Lee-Rausch, E. J. Nielson, M. A. Park, C. L. Rumsey, J. L. Thomas, K. B. Thompson, W. A. Wood, FUN3D Manual: 13.6, Technical Report NASA Technical Memorandum (TM) 2019-220416, NASA Langley Research Center, Hampton, VA, USA, 2019. URL: https://fun3d.larc.nasa.gov/papers/FUN3D_Manual-13.6.pdf.

[24] W. E. Hart, C. D. Laird, J.-P. Watson, D. L. Woodruff, G. A. Hackebeil, B. L. Nicholson, J. D. Siirola, Pyomo – optimization modeling in Python, Springer Optimization and Its Applications, 2 ed., Springer Cham, Cham, Switzerland, 2017. doi:10.1007/978-3-319-58821-6.

[25] B. Xin, L. Chen, J. Chen, H. Ishibuchi, K. Hirota, B. Liu, Interactive multiobjective optimization: A review of the state-of-the-art, *IEEE Access* 6 (2018) 41256–41279. doi:10.1109/ACCESS.2018.2856832.

[26] S. R. Hunter, E. A. Applegate, V. Arora, B. Chong, An introduction to multiobjective simulation optimization, *ACM Transactions on Modeling and Computer Simulation* 29 (2019) 1–36. doi:10.1145/3299872.

[27] J. Larson, M. Menickelly, S. M. Wild, Derivative-free optimization methods, *Acta Numerica* 28 (2019) 287–404. doi:10.1017/S0962492919000060.

[28] G. Eichfelder, Scalarizations for adaptively solving multi-objective optimization problems, *Computational Optimization and Applications* 44 (2009) 249–273. doi:10.1007/s10589-007-9155-4.

[29] A. P. Wierzbicki, Reference point approaches, in: T. Gal, T. J. Stewart, T. Hanne (Eds.), *Multicriteria Decision Making: Advances in MCDM Models, Algorithms, Theory, and Applications*, Springer US, Boston, MA, 1999, pp. 237–275. doi:10.1007/978-1-4615-5025-9_9.

[30] B. Dandurand, M. M. Wiecek, Quadratic scalarization for decomposed multiobjective optimization, *OR Spectrum* 38 (2016) 1071–1096. doi:10.1007/s00291-016-0453-z.

[31] K. Bringmann, T. Friedrich, Approximation quality of the hypervolume indicator, *Artificial Intelligence* 195 (2013) 265–290. doi:10.1016/j.artint.2012.09.005.

[32] K. Shang, H. Ishibuchi, L. He, L. M. Pang, A survey on the hypervolume indicator in evolutionary multiobjective optimization, *IEEE Transactions on Evolutionary Computation* 25 (2020) 1–20. doi:10.1109/TEVC.2020.3013290.

[33] I. Das, J. E. Dennis, Normal-boundary intersection: A new method for generating the Pareto surface in nonlinear multicriteria optimization problems, *SIAM Journal on Optimization* 8 (1998) 631–657. doi:10.1137/S1052623496307510.

[34] S. Deshpande, L. T. Watson, R. A. Canfield, Multiobjective optimization using an adaptive weighting scheme, *Optimization Methods and Software* 31 (2016) 110–133. doi:10.1080/10556788.2015.1048861.

[35] M. Laumanns, L. Thiele, E. Zitzler, An efficient, adaptive parameter variation scheme for metaheuristics based on the epsilon-constraint method, *European Journal of Operational Research* 169 (2006) 932–942. doi:10.1016/j.ejor.2004.08.029.

[36] C. Audet, J. Bégin, D. Cartier, S. Le Digabel, L. Salomon, Performance indicators in multiobjective optimization, *European Journal of Operational Research* 292 (2021) 397–422. doi:10.1016/j.ejor.2020.11.016.

[37] T. H. Chang, Mathematical Software for Multiobjective Optimization Problems, Ph.D. thesis, Virginia Tech, Dept. of Computer Science, 2020a. URL: <https://vtworks.lib.vt.edu/handle/10919/98915>.

[38] E. Bradford, A. M. Schweidtmann, A. Lapkin, Efficient multiobjective optimization employing Gaussian processes, spectral sampling and a genetic algorithm, *Journal of Global Optimization* 71 (2018) 407–438. doi:10.1007/s10898-018-0609-2.

[39] T. H. Chang, L. T. Watson, J. Larson, N. Neveu, W. I. Thacker, S. Deshpande, T. C. H. Lux, Algorithm 1028: VTMOP: Solver for blackbox multiobjective optimization problems, *ACM Transactions on Mathematical Software* 48 (2022) Article No. 36. doi:10.1145/3529258.

[40] J. Müller, SOCEMO: Surrogate optimization of computationally expensive multiobjective problems, *INFORMS Journal on Computing* 29 (2017) 581–596. doi:10.1287/ijoc.2017.0749.

[41] J. Thomann, G. Eichfelder, A trust-region algorithm for heterogeneous multiobjective optimization, *SIAM Journal on Optimization* 29 (2019) 1017–1047. doi:10.1137/18m1173277.

[42] M. A. Bouhlel, J. T. Hwang, N. Bartoli, R. Lafage, J. Morlier, J. R. Martins, A Python surrogate modeling framework with derivatives, *Advances in Engineering Software* 135 (2019) 102–662. doi:10.1016/j.advengsoft.2019.03.005.

[43] M. Balandat, B. Karrer, D. Jiang, S. Daulton, B. Letham, A. G. Wilson, E. Bakshy, BoTorch: A framework for efficient Monte-Carlo Bayesian optimization, *Advances in Neural Information Processing Systems* 33 (2020) 21524–21538. URL: <https://proceedings.neurips.cc/paper/2020/file/f5b1b89d98b7286673128a5fb112cb9a-Paper.pdf>.

[44] M. Emmerich, K. Yang, A. Deutz, H. Wang, C. M. Fonseca, A multicriteria generalization of Bayesian global optimization, in: P. M. Pardalos, A. Zhigljavsky, J. Žilinskas (Eds.), *Advances in Stochastic and Deterministic Global Optimization*, Springer, 2016, pp. 229–242. doi:10.1007/978-3-319-29975-4.

[45] P. Feliot, J. Bect, E. Vazquez, A Bayesian approach to constrained single- and multi-objective optimization, *Journal of Global Optimization* 67 (2016) 97–133. doi:10.1007/s10898-016-0427-3.

[46] B. M. Adams, W. J. Bohnhoff, K. R. Dalbey, M. S. Ebeida, J. P. Eddy, M. S. Eldred, R. W. Hooper, P. D. Hough, K. T. Hu, J. D. Jakeman, M. Khalil, K. A. Maupin, J. A. Monschke, E. M. Ridgeway, A. A. Rushdi, D. T. Seidl, J. A. Stephens, L. P. Swiler, A. Tran, J. G. Winokur, Dakota, A Multilevel Parallel Object-Oriented Framework for Design Optimization, Parameter Estimation, Uncertainty Quantification, and Sensitivity Analysis: Version 6.16 User's Manual, Technical Report SAND2022-6171 version 6.16, Sandia National Laboratory, Albuquerque, NM, USA, 2022. URL: <https://dakota.sandia.gov/sites/default/files/docs/6.16.0/Users-6.16.0.pdf>.

[47] S. Balay, S. Abhyankar, M. F. Adams, S. Benson, J. Brown, P. Brune, K. Buschelman, E. Constantinescu, L. Dalcin, A. Dener, V. Eijkhout, W. D. Gropp, V. Hapla, T. Isaac, P. Jolivet, D. Karpeev, D. Kaushik, M. G. Knepley, F. Kong, S. Kruger, D. A. May, L. C. McInnes, R. T. Mills, L. Mitchell, T. Munson, J. E. Roman, K. Rupp, P. Sanan, J. Sarich, B. F. Smith, S. Zampini, H. Zhang, H. Zhang, J. Zhang, PETSc/TAO Users Manual, Technical Report ANL-21/39 - Revision 3.19, Argonne National Laboratory, Lemont, IL, USA, 2023. URL: <https://petsc.org/release/docs/manual/manual.pdf>.

[48] A. Dener, A. Denchfield, H. Suh, T. Munson, J. Sarich, S. Wild, S. Benson, L. C. McInnes, TAO Users Manual, Technical Report ANL/MCS-TM-322 Rev. 3.15, Argonne National Laboratory, Lemont, IL, USA, 2021. doi:10.2172/1814593.

[49] J. S. Gray, J. T. Hwang, J. R. Martins, K. T. Moore, B. A. Naylor, OpenMDAO: An open-source framework for multidisciplinary design, analysis, and optimization, *Structural and Multidisciplinary Optimization* 59 (2019) 1075–1104. doi:10.1007/s00158-019-02211-z.

[50] R. M. Kolonay, M. Sobolewski, Service oriented computing environment (SORCER) for large scale, distributed, dynamic fidelity aeroelastic analysis, in: International Forum on Aeroelasticity and Structural Dynamics (IFASD 2011), Citeseer, 2011, pp. 26–30. URL: <http://citeseerx.ist.psu.edu/viewdoc/summary?doi=10.1.1.656.7539>.

[51] J. R. R. A. Martins, C. Marriage, N. Tedford, pyMDO: An object-oriented framework for multidisciplinary design optimization, *ACM Transactions on Mathematical Software* 36 (2009) Article No. 20. doi:10.1145/1555386.1555389.

[52] G. E. Karniadakis, I. G. Kevrekidis, L. Lu, P. Perdikaris, S. Wang, L. Yang, Physics-informed machine learning, *Nature Reviews Physics* 3 (2021) 422–440. doi:10.1038/s42254-021-00314-5.

[53] S. S. Garud, I. A. Karimi, M. Kraft, Smart sampling algorithm for surrogate model development, *Computers & Chemical Engineering* 96 (2017) 103–114. doi:10.1016/j.compchemeng.2016.10.006.

[54] H. Liu, J. Cai, Y.-S. Ong, An adaptive sampling approach for kriging metamodeling by maximizing expected prediction error, *Computers & Chemical Engineering*, Special Section - ESCAPE-26 106 (2017) 171–182. doi:10.1016/j.compchemeng.2017.05.025.

[55] S. M. Wild, Solving derivative-free nonlinear least squares problems with POUNDERS, in: T. Terlaky, M. F. Anjos, S. Ahmed (Eds.), *Advances and Trends in Optimization with Engineering Applications*, SIAM, 2017, pp. 529–540. doi:10.1137/1.9781611974683.ch40.

[56] K. A. Khan, J. Larson, S. M. Wild, Manifold sampling for optimization of nonconvex functions that are piecewise linear compositions of smooth components, *SIAM Journal on Optimization* 28 (2018) 3001–3024. doi:10.1137/17m114741x.

[57] J. Blank, K. Deb, *pymoo: Multi-objective optimization in Python*, *IEEE Access* 8 (2020) 89497–89509. doi:10.1109/ACCESS.2020.2990567.

[58] S. Le Digabel, Algorithm 909: NOMAD: Nonlinear optimization with the MADS algorithm, *ACM Transactions on Mathematical Software* 37 (2011) Article No. 44. doi:10.1145/1916461.1916468.

[59] L. Luo, T. P. Straatsma, L. E. A. Suarez, R. Broer, D. Bykov, E. F. D’Azevedo, S. S. Faraji, K. C. Gottiparthi, C. De Graaf, J. A. Harris, R. W. A. Havenith, H. J. A. Jensen, W. Joubert, R. K. Kathir, J. Larkin, Y. W. Li, D. I. Lyakh, O. E. B. Messer, M. R. Norman, J. C. Oefelein, R. Sankaran, A. F. Tillack, A. L. Barnes, L. Visscher, J. C. Wells, M. Wibowo, Pre-exascale accelerated application development: The ORNL Summit experience, *IBM Journal of Research and Development* 64 (2020) 11:1–11:21. doi:10.1147/JRD.2020.2965881.

[60] A. Lavely, Powering Extreme-Scale HPC with Cerebras Wafer-Scale Accelerators, Technical Report, Cerebras Systems, Inc., Sunnyvale, CA, USA, 2022. URL: <https://8968533.fs1.hubspotusercontent-na1.net/hubfs/8968533/Powering-Extreme-Scale-HPC-with-Cerebras.pdf>.

[61] T. Louw, S. McIntosh-Smith, Using the Graphcore IPU for traditional HPC applications, in: Proc. 3rd Workshop on Accelerated Machine Learning (AccML), 2021, pp. 1–9. URL: <https://easychair.org/publications/preprint/ztfj>.

[62] A. Dubey, L. C. McInnes, R. Thakur, E. W. Draeger, T. Evans, T. C. Germann, W. E. Hart, Performance portability in the Exascale Computing Project: Exploration through a panel series, *Computing in Science & Engineering* 23 (2021) 46–54. doi:10.1109/MCSE.2021.3098231.

[63] R. T. Mills, M. F. Adams, S. Balay, J. Brown, A. Dener, M. Knepley, S. E. Kruger, H. Morgan, T. Munson, K. Rupp, B. F. Smith, S. Zampini, H. Zhang, J. Zhang, Toward performance-portable PETSc for GPU-based exascale systems, *Parallel Computing* 108 (2021) 102831. doi:10.1016/j.parco.2021.102831.

[64] R. Chard, Y. Babuji, Z. Li, T. Skluzacek, A. Woodard, B. Blaiszik, I. Foster, K. Chard, funcX: A federated function serving fabric for science, in: Proc. 29th International Symposium on High-Performance Parallel and Distributed Computing (HPDC ’20), ACM, 2020, pp. 65–76. doi:10.1145/3369583.3392683.

[65] S. Hudson, J. Larson, S. M. Wild, D. Bindel, J.-L. Navarro, libEnsemble Users Manual, Technical Report Revision 0.9.1, Argonne National Laboratory, Lemont, IL, USA, 2022a. URL: <https://buildmedia.readthedocs.org/media/pdf/libensemble/latest/libensemble.pdf>.

[66] S. Hudson, J. Larson, J.-L. Navarro, S. M. Wild, libEnsemble: A library to coordinate the concurrent evaluation of dynamic ensembles of calculations, *IEEE Transactions on Parallel and Distributed Systems* 33 (2022b) 977–988. doi:10.1109/tpds.2021.3082815.

[67] T. H. Chang, J. Larson, L. T. Watson, T. C. H. Lux, Managing computationally expensive blackbox multiobjective optimization problems using libEnsemble, in: Proc. 2020 Spring Simulation Conference (SpringSim 2020), the 28th High Performance Computing Symposium (HPC ’20), SCS, 2020b, p. Article No. 31. doi:10.22360/SpringSim.2020.HPC.001.

[68] C. Raghunath, T. H. Chang, L. T. Watson, M. Jrad, R. K. Kapania, R. M. Kolonay, Global deterministic and stochastic optimization in a service oriented architecture, in: Proc. 2017 Spring Simulation Conference (SpringSim 2017), the 25th High Performance Computing Symposium (HPC '17), SCS, Virginia Beach, VA, USA, 2017, p. Article No. 7. doi:10.22360/springsim.2017.hpc.023.

[69] S. Stall, L. Yarmey, J. Cutcher-Gershenfeld, B. Hanson, K. Lehnert, B. Nosek, M. Parsons, E. Robinson, L. Wyborn, Make scientific data FAIR, *Nature* 570 (2019) 27–29. doi:10.1038/d41586-019-01720-7.

[70] M. Barker, N. P. Chue Hong, D. S. Katz, A.-L. Lamprecht, C. Martinez-Ortiz, F. Psomopoulos, J. Harrow, L. J. Castro, M. Gruenpeter, P. A. Martinez, T. Honeyman, Introducing the FAIR principles for research software, *Scientific Data* 9 (2022) Article No. 622. doi:10.1038/s41597-022-01710-x.

[71] M. A. Heroux, L. McInnes, D. E. Bernholdt, A. Dubey, E. Gonsiorowski, O. Marques, J. D. Moulton, B. Norris, E. Raybourn, S. Balay, R. A. Bartlett, L. Childers, T. Gamblin, P. Grubel, R. Gupta, R. Hartman-Baker, J. C. Hill, S. Hudson, C. Junghans, A. Klinvex, R. Milewicz, M. Miller, H. Ah Nam, J. O’Neal, K. Riley, B. Sims, J. Schuler, B. F. Smith, L. Vernon, G. R. Watson, J. Willenbring, P. Wolfenbarger, Advancing Scientific Productivity through Better Scientific Software: Developer Productivity and Software Sustainability Report, Technical Report ORNL TM-2020 1459 / ECP-U-RPT-2020-0001, Oak Ridge National Laboratory, Oak Ridge, TN, USA, 2020. doi:10.2172/1606662.

[72] T. M. Ragonneau, Z. Zhang, PDFO: a cross-platform package for Powell’s derivative-free optimization solvers, Technical Report, arXiv preprint, 2023. doi:10.48550/arXiv.2302.13246.

[73] C. Audet, S. Le Digabel, V. Rochon Montplaisir, C. Tribes, Algorithm 1027: NOMAD version 4: Nonlinear optimization with the MADS algorithm, *ACM Transactions on Mathematical Software* 48 (2022). doi:10.1145/3544489.

[74] A. Benítez-Hidalgo, A. J. Nebro, J. García-Nieto, I. Oregi, J. Del Ser, jMetalPy: A Python framework for multi-objective optimization with metaheuristics, *Swarm and Evolutionary Computation* 51 (2019) 100598. doi:10.1016/j.swevo.2019.100598.

[75] E. Zitzler, M. Laumanns, L. Thiele, SPEA2: Improving the strength Pareto evolutionary algorithm, TIK-report 103 (2001). doi:10.3929/ethz-a-004284029.

[76] K. Deb, A. Pratap, S. Agarwal, T. Meyarivan, A fast and elitist multiobjective genetic algorithm: NSGA-II, *IEEE Transactions on Evolutionary Computation* 6 (2002a) 182–197. doi:10.1109/4235.996017.

[77] D. Hadka, Platypus – multiobjective optimization in Python, Technical Report Version 1.0.4, GitHub, 2015. URL: <https://platypus.readthedocs.io/en/latest>.

[78] Y. Tian, R. Cheng, X. Zhang, Y. Jin, PlatEMO: A MATLAB platform for evolutionary multi-objective optimization [educational forum], *IEEE Computational Intelligence Magazine* 12 (2017) 73–87. doi:10.1109/MCI.2017.2742868.

[79] J. J. Durillo, A. J. Nebro, jMetal: A Java framework for multi-objective optimization, *Advances in Engineering Software* 42 (2011) 760–771. doi:10.1016/j.advengsoft.2011.05.014.

[80] F. Biscani, D. Izzo, A parallel global multiobjective framework for optimization: pagmo, *Journal of Open Source Software* 5 (2020) 2338. doi:10.21105/joss.02338.

[81] F.-A. Fortin, F.-M. De Rainville, M.-A. Gardner, M. Parizeau, C. Gagné ”, DEAP: Evolutionary algorithms made easy, *Journal of Machine Learning Research* 13 (2012) 2171–2175. URL: <https://www.jmlr.org/papers/v13/fortin12a.html>.

[82] S. Tavares, C. P. Brás, A. L. Custódio, V. Duarte, P. Medeiros, Parallel strategies for direct multisearch, *Numerical Algorithms* 92 (2022) 1757–1788. doi:10.1007/s11075-022-01364-1.

[83] K. Cooper, S. R. Hunter, PyMOSO: Software for multi-objective simulation optimization with R-PERLE and R-MinRLE, *INFORMS Journal on Computing* 32 (2020) 1101–1108. doi:10.1287/ijoc.2019.0902.

[84] A. Paszke, S. Gross, F. Massa, A. Lerer, J. Bradbury, G. Chanan, T. Killeen, Z. Lin, N. Gimelshein, L. Antiga, A. Desmaison, A. Kopf, E. Yang, Z. DeVito, M. Raison, A. Tejani, S. Chilamkurthy, B. Steiner, L. Fang, J. Bai, S. Chintala, PyTorch: An imperative style, high-performance deep learning library, *Advances in Neural Information Processing Systems* 32 (2019) 1–12. URL: <https://proceedings.neurips.cc/paper/2019/file/bdbca288fee7f92f2bfa9f7012727740-Paper.pdf>.

[85] T. H. Chang, S. M. Wild, H. Dickinson, ParMOO: Python library for parallel multiobjective simulation optimization, Technical Report Version 0.2.0, Argonne National Laboratory, Lemont, IL, USA, 2023a. URL: <https://parmoo.readthedocs.io/en/latest>.

[86] I. Dunning, J. Huchette, M. Lubin, JuMP: A modeling language for mathematical optimization, *SIAM Review* 59 (2017) 295–320. doi:10.1137/15M1020575.

[87] D. Eriksson, M. Pearce, J. Gardner, R. D. Turner, M. Poloczek, Scalable global optimization via local bayesian optimization, *Advances in Neural Information Processing Systems* 32 (2019) 1–12. URL: <https://proceedings.neurips.cc/paper/2019/file/6c990b7aca7bc7058f5e98ea909e924b-Paper.pdf>.

[88] J. Larson, M. Menickelly, Structure-Aware Methods for Expensive Derivative-Free Nonsmooth Composite Optimization, Technical Report, arXiv preprint, 2022. doi:10.48550/arXiv:2207.08264.

[89] H. Zhang, A. R. Conn, On the local convergence of a derivative-free algorithm for least-squares minimization, *Computational Optimization and Applications* 51 (2012) 481–507. doi:10.1007/s10589-010-9367-x.

[90] H. Moriwaki, Y.-S. Tia, N. Kawashita, T. Takagi, Mordred: a molecular descriptor calculator, *Journal of Cheminformatics* 10 (2018). doi:10.1186/s13321-018-0258-y.

[91] D. Golovin, B. Solnik, S. Moitra, G. Kochanski, J. Karro, D. Sculley, Google Vizier: A service for black-box optimization, in: Proc. 23rd ACM SIGKDD International Conference on Knowledge Discovery and Data Mining (KDD '17), ACM, 2017, p. 1487–1495. doi:10.1145/3097983.3098043.

[92] P. Saves, R. Lafage, N. Bartoli, Y. Diouane, J. Bussemaker, T. Lefebvre, J. T. Hwang, J. Morlier, J. R. R. A. Martins, SMT 2.0: A Surrogate Modeling Toolbox with a focus on Hierarchical and Mixed Variables Gaussian Processes, Technical Report, arXiv preprint, 2023. doi:10.48550/arXiv.2305.13998.

[93] F. Chollet, et al., Keras, <https://keras.io>, 2015.

[94] C. Zhu, R. H. Byrd, P. Lu, J. Nocedal, Algorithm 778: L-BFGS-B: Fortran subroutines for large-scale bound-constrained optimization, *ACM Transactions on Mathematical Software* 23 (1997) 550–560. doi:10.1145/279232.279236.

[95] P. Virtanen, R. Gommers, T. E. Oliphant, M. Haberland, T. Reddy, D. Cournapeau, E. Burovski, P. Peterson, W. Weckesser, J. Bright, S. J. van der Walt, M. Brett, J. Wilson, K. Jarrod Millman, N. Mayorov, A. R. J. Nelson, E. Jones, R. Kern, E. Larson, C. Carey, İ. Polat, Y. Feng, E. W. Moore, J. VanderPlas, D. Laxalde, J. Perktold, R. Cimrman, I. Henriksen, E. A. Quintero, C. R. Harris, A. M. Archibald, A. H. Ribeiro, F. Pedregosa, P. van Mulbregt, et al., SciPy 1.0: Fundamental algorithms for scientific computing in Python, *Nature Methods* 17 (2020) 261–272. doi:10.1038/s41592-019-0686-2.

[96] T. H. Chang, J. R. Elias, S. M. Wild, S. Chaudhuri, J. A. Libera, A framework for fully autonomous design of materials via multiobjective optimization and active learning: challenges and next steps, in: 11th Intl. Conf. on Learning Representation (ICLR 2023), Workshop on Machine Learning for Materials (ML4Materials), 2023c, pp. 1–10. URL: <https://openreview.net/forum?id=8KJS7RPjMqG>, to appear.

[97] F. Pedregosa, G. Varoquaux, A. Gramfort, V. Michel, B. Thirion, O. Grisel, M. Blondel, P. Prettenhofer, R. Weiss, V. Dubourg, et al., Scikit-learn: Machine learning in Python, *Journal of Machine Learning Research* 12 (2011) 2825–2830. URL: <https://www.jmlr.org/papers/volume12/pedregosa11a/pedregosa11a.pdf>.

The submitted manuscript has been created by UChicago Argonne, LLC, Operator of Argonne National Laboratory (“Argonne”). Argonne, a U.S. Department of Energy Office of Science laboratory, is operated under Contract No. DE-AC02-06CH11357. The U.S. Government retains for itself, and others acting on its behalf, a paid-up nonexclusive, irrevocable worldwide license in said article to reproduce, prepare derivative works, distribute copies to the public, and perform publicly and display publicly, by or on behalf of the Government. The Department of Energy will provide public access to these results of federally sponsored research in accordance with the DOE Public Access Plan. <http://energy.gov/downloads/doe-public-access-plan>